The Astrophysical Journal, 753:30 (18pp), 2012 July 1 doi:10.1088/0004-637X/753/1/30

MID-INFRARED SELECTION OF ACTIVE GALACTIC NUCLEI WITH THE *WIDE-FIELD INFRARED SURVEY EXPLORER*. I. CHARACTERIZING *WISE*-SELECTED ACTIVE GALACTIC NUCLEI IN COSMOS

Daniel Stern[1], Roberto J. Assef[1,10], Dominic J. Benford[2], Andrew Blain[3], Roc Cutri[4], Arjun Dey[5], Peter Eisenhardt[1], Roger L. Griffith[4], T. H. Jarrett[4], Sean Lake[6], Frank Masci[4], Sara Petty[6], S. A. Stanford[7,8], Chao-Wei Tsai[4], E. L. Wright[6], Lin Yan[4], Fiona Harrison[9], and Kristin Madsen[9]
[1] Jet Propulsion Laboratory, California Institute of Technology, 4800 Oak Grove Drive, Mail Stop 169-221, Pasadena, CA 91109, USA; daniel.k.stern@jpl.nasa.gov
[2] NASA Goddard Space Flight Center, Code 665, Greenbelt, MD 20771, USA
[3] Department of Physics and Astronomy, University of Leicester, LE1 7RH Leicester, UK
[4] Infrared Processing and Analysis Center, California Institute of Technology, Pasadena, CA 91125, USA
[5] National Optical Astronomical Observatory, 950 N. Cherry Ave., Tucson, AZ 85719, USA
[6] Physics and Astronomy Department, University of California, Los Angeles, CA 90095, USA
[7] Department of Physics, University of California, One Shields Avenue, Davis, CA 95616, USA
[8] Institute of Geophysics and Planetary Physics, Lawrence Livermore National Laboratory, Livermore, CA 94550, USA
[9] Space Radiation Laboratory, California Institute of Technology, Pasadena, CA 91125, USA
Received 2011 November 2; accepted 2012 April 24; published 2012 June 12

ABSTRACT

The *Wide-field Infrared Survey Explorer* (*WISE*) is an extremely capable and efficient black hole finder. We present a simple mid-infrared color criterion, $W1 - W2 \geqslant 0.8$ (i.e., $[3.4]-[4.6] \geqslant 0.8$, Vega), which identifies 61.9 ± 5.4 active galactic nucleus (AGN) candidates per deg^2 to a depth of $W2 \sim 15.0$. This implies a much larger census of luminous AGNs than found by typical wide-area surveys, attributable to the fact that mid-infrared selection identifies both unobscured (type 1) and obscured (type 2) AGNs. Optical and soft X-ray surveys alone are highly biased toward only unobscured AGNs, while this simple *WISE* selection likely identifies even heavily obscured, Compton-thick AGNs. Using deep, public data in the COSMOS field, we explore the properties of *WISE*-selected AGN candidates. At the mid-infrared depth considered, 160 μJy at 4.6 μm, this simple criterion identifies 78% of *Spitzer* mid-infrared AGN candidates according to the criteria of Stern et al. and the reliability is 95%. We explore the demographics, multiwavelength properties and redshift distribution of *WISE*-selected AGN candidates in the COSMOS field.

Key words: galaxies: active – infrared: galaxies

Online-only material: color figure

1. INTRODUCTION

Most surveys for active galactic nuclei (AGNs) are severely biased toward unobscured (type 1) AGNs. Nuclear emission in such sources dominates over host galaxy light at most wavelengths, making type 1 AGNs both more readily identifiable and easier to follow-up spectroscopically. However, models predict a large population of obscured (type 2) AGNs, outnumbering type 1 AGNs by a factor of ∼3 (e.g., Comastri et al. 1995; Treister et al. 2004; Ballantyne et al. 2011). Determining the ratio of unobscured to obscured AGNs as a function of luminosity and redshift has direct implications for the growth history of supermassive black holes in galactic centers, as well as for the origin of the cosmic X-ray background (and, at a ∼10% level, optical and infrared backgrounds). Furthermore, recent theoretical work suggests that AGN feedback plays a dominant role in establishing the present-day appearances of galaxies (e.g., Silk & Rees 1998; Hopkins et al. 2008). With the dominant population of obscured AGN severely underrepresented by current studies, however, a full understanding of the interplay between AGN feedback and galaxy formation is hampered.

The most promising photometric techniques for identifying luminous type 2 AGNs are radio selection, hard X-ray selection, and mid-infrared selection. However, only ∼10% of AGNs are radio loud (e.g., Stern et al. 2000b) and the current generation of hard X-ray satellites have limited sensitivity. Specifically, recent surveys with *Swift* and *INTEGRAL* have only identified a few dozen heavily obscured (e.g., Compton-thick) AGNs, all at very low redshift, $z \approx 0$ (e.g., Bassani et al. 1999; Vignali & Comastri 2002; Ajello et al. 2008; Tueller et al. 2008; Burningham et al. 2011). The *Nuclear Spectroscopic Telescope Array* (*NuSTAR*; Harrison et al. 2010), scheduled for launch in 2012 June, will improve that hard X-ray (∼30 keV) sensitivity by a factor of ∼200, but with a field of view (FoV) comparable to *Chandra*/ACIS, *NuSTAR* will only undertake a limited number of extragalactic surveys, unlikely to cover more than a few square degrees of sky. With mid-infrared sensitivities several orders of magnitude greater than the *Infrared Astronomical Satellite*, the *Wide-field Infrared Survey Explorer* (*WISE;* Wright et al. 2010) promises the first sensitive full-sky survey for both type 1 and type 2 luminous AGNs.

WISE launched on UT 2009 December 14 and completed its first survey of the entire sky on UT 2010 July 17, obtaining a minimum coverage of five exposures per sky position over 95% of the sky in four passbands, 3.4, 4.6, 12, and 22 μm ($W1$, $W2$, $W3$, and $W4$). The all-sky data release occurred on 2012 March 14, releasing all data taken during the *WISE* full cryogenic mission phase.[11] The median depth-of-coverage is 15.6 exposures per sky position for $W1$ and $W2$, and 14.8 exposures per sky position for $W3$ and $W4$. Accounting for source confusion, the estimated sensitivities are 0.068, 0.098, 0.86, and 5.4 mJy (5σ), respectively (Wright et al. 2010).

[10] NASA Postdoctoral Program Fellow.

[11] See http://wise2.ipac.caltech.edu/docs/release/allsky/.

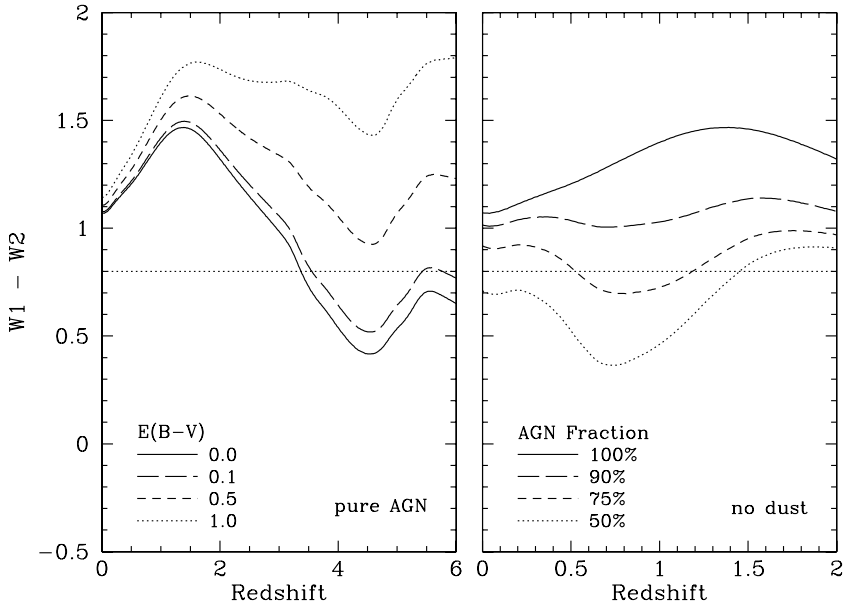

Figure 1. Model colors of AGNs as a function of redshift using the templates of Assef et al. (2010; Vega magnitudes). The left panel shows a pure AGN template with increasing amounts of dust extinction. The right panel shows an unextincted AGN diluted by increasing amounts of host galaxy light, where the host is the early-type (E) template from Assef et al. (2010); changing the galaxy template has minimal effect. A simple color criterion of $W1 - W2 \geqslant 0.8$ identifies pure AGNs out to $z \sim 3$ and extincted pure AGNs out to higher redshifts. For unextincted AGNs, sources are no longer selected as the host galaxy becomes an increasing fraction of the bolometric luminosity.

The corresponding Vega magnitude limits are 16.83, 15.60, 11.32, and 8.0, respectively. The depth increases with ecliptic latitude, reaching more than five times greater sensitivity near the ecliptic poles (Jarrett et al. 2011). In order of increasing wavelength, the imaging resolution (FWHM) is 6.″1, 6.″4, 6.″5, and 12.″0 for the four bands.

Similar to the UV-excess method of identifying quasars (e.g., Schmidt & Green 1983), mid-infrared selection of AGNs relies on distinguishing the approximately power-law AGN spectrum from the blackbody stellar spectrum of galaxies which peaks at rest frame 1.6 μm. Mid-infrared data easily separate AGNs from stars and galaxies, with the added benefit that mid-infrared selection is less susceptible to dust extinction and is sensitive to the highest redshift sources. Courtesy of the unprecedented sensitivity and mapping efficiency of the Infrared Array Camera (IRAC; Fazio et al. 2004) on board the *Spitzer Space Telescope*, the past few years have seen an explosion of research using mid-infrared observations to find and study (obscured) AGNs at high redshift (e.g., Lacy et al. 2004, 2007; Stern et al. 2005; Alonso-Herrero et al. 2006; Barmby et al. 2006; Martínez-Sansigre et al. 2006, 2007; Donley et al. 2007, 2008, 2012; Dey et al. 2008; Fiore et al. 2008, 2009; Hatziminaoglou et al. 2008; Rigopoulou et al. 2009; Seymour et al. 2007; De Breuck et al. 2010; Eckart et al. 2010; Park et al. 2010). IRAC identification of AGNs typically required all four passbands of that instrument, with data out to 8 μm, to differentiate AGNs from high-redshift ($z \gtrsim 1.3$) massive galaxies. This is because distant, massive galaxies have red observed colors from 3 to 5 μm (e.g., Lacy et al. 2004; Stern et al. 2005; Donley et al. 2007, 2012; Hickox et al. 2009; Galametz et al. 2012) and even very shallow (<90 s) IRAC pointings easily reach well below the characteristic brightness of early-type galaxies out to $z \sim 2$, $m^*_{4.5} \approx 16.7$ (e.g., Mancone et al. 2010). Because of its shallow observations, *WISE* suffers less pronouncedly from such contamination and therefore is able to robustly identify AGNs with just the two bluest, most sensitive channels.

Figure 1 illustrates *WISE* selection of AGNs. As anticipated prior to the launch of *WISE* in Ashby et al. (2009), Assef et al. (2010), and Eckart et al. (2010), a simple $W1 - W2$ color cut robustly differentiates AGNs from stars and galaxies. Since the public release of *WISE* data, several teams have also noted the efficiency with which *WISE* identifies AGNs (e.g., D'Abrusco et al. 2012; Edelson & Malkan 2012; Massaro et al. 2012), though these analyses have used the full four-band *WISE* photometry. Using the empirical AGNs and galaxy spectral templates of Assef et al. (2010), Figure 1 shows how $W1 - W2$ color evolves with redshift. The left panel considers a pure AGN template with increasing amounts of dust extinction while the right panel considers an unobscured AGN increasingly diluted by stellar emission (modeled with the elliptical galaxy, or E, template). AGN fraction refers to the fraction of the integrated emission in the rest-frame 0.1–30 μm range of the unextincted templates which comes from the AGN.

Out to $z \sim 3.5$, pure AGNs have red $W1 - W2$ mid-infrared colors. Beyond this redshift, the templates become blue as the $\sim$1 μm minimum in the AGN template shifts into the $W2$ band (see also Richards et al. 2006a). Hα emission shifting into the $W1$ band plays an additional role in causing blue $W1 - W2$ colors for AGNs at $z \gtrsim 3.4$ (Assef et al. 2010). Even modest amounts of dust extinction redden the observed $W1 - W2$ colors for high-redshift AGNs. Heavily extincted pure AGNs are extremely red; for example, a pure AGN reddened by $E(B-V) = 15$ has $W1 - W2 > 2$ at all redshifts. Mid-infrared selection of AGNs is remarkably robust at identifying pure AGNs regardless of redshift. Indeed, Blain et al. (2012) report on the *WISE* detection of many of the highest redshift, $z > 6$, quasars known, including the recently discovered $z = 7.085$ quasar from the United Kingdom Infrared Deep Sky Survey (Mortlock et al. 2011). That quasar, the most distant currently known, has $W1 - W2 \sim 1.2$.

In contrast, normal galaxies and Galactic sources are unlikely to present such red $W1 - W2$ colors. The galaxy templates of

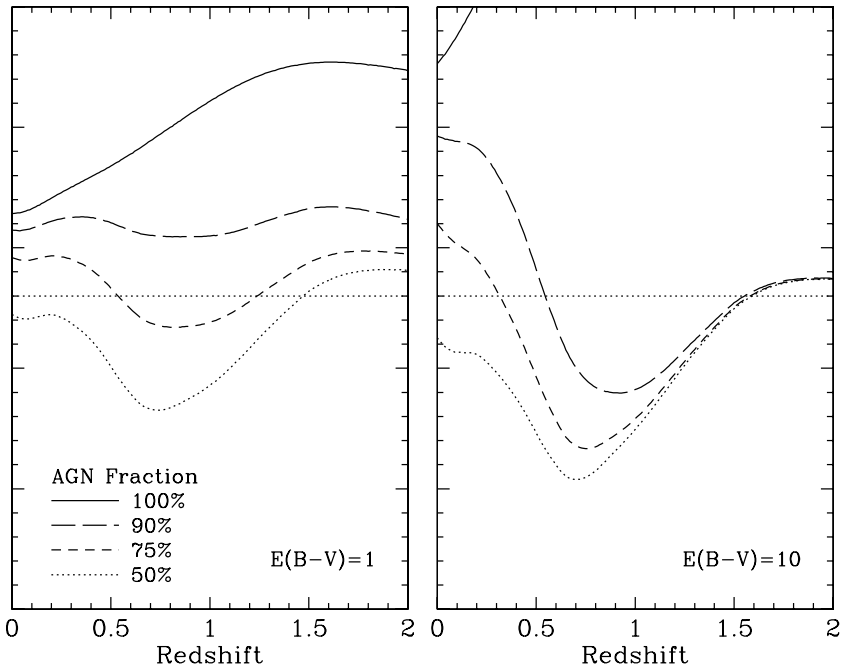

Figure 2. Model colors of an extincted AGN as a function of redshift for increasing contributions of host galaxy light. As per Figure 1, models use the AGN and early-type (E) galaxy template of Assef et al. (2010; Vega magnitudes); changing the galaxy template has minimal effect. The left panel shows a modestly extincted AGN with $E(B-V)=1$, corresponding to $N_{\rm H}\sim 6\times10^{22}\,{\rm cm}^{-2}$, while the right panels show a heavily extincted AGN with $E(B-V)=10$, corresponding to $N_{\rm H}\sim 6\times10^{23}\,{\rm cm}^{-2}$. For modest levels of extinction, the results are essentially unchanged from the right panel of Figure 1: a simple color criterion of $W1-W2\geqslant 0.8$ identifies AGN-dominated galaxies so long as the AGN fraction is $\gtrsim$80%. For heavily extincted AGNs, including Compton-thick AGNs ($N_{\rm H}\gtrsim 10^{24}\,{\rm cm}^{-2}$), the mid-infrared emission becomes dominated by the host galaxy above redshifts of a few tenths, essentially regardless of AGN fraction, making it difficult to distinguish such systems from normal galaxies using just $W1-W2$ color.

Assef et al. (2010) are blue in this *WISE* color combination, with $W1-W2\leqslant 0.8$ out to $z\sim 1.2$. Given the shallow sensitivity of *WISE*, only the tip of the galaxy luminosity function will be well detected by *WISE* at higher redshifts, particularly when the analysis is restricted to the very conservative 10σ flux limit ($W2\sim 15.0$) we apply in this paper. In terms of Galactic contamination, only the coolest brown dwarfs and the most heavily dust-reddened stars will exhibit such red *WISE* colors. Kirkpatrick et al. (2011) show that stars of spectral class later (e.g., cooler) than ~T1 have $W1-W2\geqslant 0.8$; these red colors are caused by methane absorption in the $W1$ band (see also Cushing et al. 2011). In a high Galactic latitude survey, neither cool brown dwarfs nor dust-reddened stars will be significant contaminants at the flux limit of *WISE*.

As seen in the right panel of Figure 1, dilution by the host galaxy will cause blue $W1-W2$ colors, making less powerful AGNs no longer identifiable using this simple *WISE* color criterion. This illustrates a synergy between X-ray and mid-infrared surveys. While sensitive soft X-ray ($\leqslant$10 keV) surveys are quite powerful at identifying even low-luminosity AGNs since stellar processes are unlikely to power X-ray emission at luminosities greater than $\sim10^{42}\,{\rm erg\,s}^{-1}$ (e.g., Stern et al. 2002b; Brandt & Hasinger 2005), such surveys are not sensitive to heavily obscured AGNs since the low energy X-rays are readily absorbed and scattered. This is particularly true for heavily obscured low-redshift sources; higher redshift obscured AGNs are helped by advantageous *k*-corrections (e.g., Stern et al. 2002a). Mid-infrared surveys, in contrast, readily identify the most heavily obscured, luminous AGNs since the obscuring material is thermally heated by the AGN and emits relatively unimpeded by dust extinction. However, dilution by the host galaxy limits mid-infrared surveys from identifying low-luminosity AGNs. Optical photometric surveys are the most heavily biased, with a sensitivity largely restricted to the least obscured, most luminous AGN. Using data from deep *Chandra* and *Spitzer* imaging of targeted surveys, significant advances have come in recent years at understanding the full census of AGNs (e.g., Polletta et al. 2006; Hickox et al. 2007; Fiore et al. 2008; Gorjian et al. 2008; Comastri et al. 2011; Hickox et al. 2011; Mullaney et al. 2011). Combining *WISE* with soft X-ray data from the all-sky eROSITA telescope on *Spectrum Röntgen Gamma* (Predehl et al. 2010), expected to launch in late 2013, will extend the results of these targeted surveys across the full sky.

How will *WISE* perform at identifying the most heavily obscured, Compton-thick AGNs? Assuming an SMC-like gas-to-dust ratio ($N_{\rm H}\sim 2\times10^{22}\,{\rm cm}^{-2}\,{\rm mag}^{-1}$; Maiolino et al. 2001), $N_{\rm H}\sim 10^{24}\,{\rm cm}^{-2}$ corresponds to $A_V\sim 50$ or $E(B-V)\sim 15$ for $R_V\sim 3.1$ (e.g., Cardelli et al. 1989; Gordon & Clayton 1998; York et al. 2006). As can be inferred from the left panel of Figure 1, such heavily obscured pure AGNs will have very red $W1-W2$ colors at any redshift. However, host galaxy dilution in these bands will become significant as extreme obscuration hides the AGN. As shown in Figure 2, the effect is subtle for modestly extincted sources with $N_{\rm H}\lesssim 6\times10^{22}\,{\rm cm}^{-2}$, corresponding to $E(B-V)\lesssim 1$. Such AGNs should be readily identifiable from their $W1-W2$ colors so long as the AGN is bolometrically dominant. However, the blue mid-infrared colors of the host stellar populations across these *WISE* bands will make low-redshift, heavily obscured AGNs difficult to identify at mid-infrared wavelengths. At higher redshifts, $z\gtrsim 1.5$, the host galaxy becomes red across these bands, but also fades below the detection limit of *WISE*. The most heavily obscured AGNs are most likely best identified using the longer wavelength *WISE* passbands. However, the cost is that the diminished sensitivity of those bands limits searches to the most luminous

sources. Indeed, Eisenhardt et al. (2012) report on a *WISE*-selected source which is undetected in $W1$ and $W2$, but has very red $W2-W3$ colors. Similarly selected sources are further discussed in Bridge et al. (2012) and Wu et al. (2012); we find only ∼1000 such extreme sources across the full sky.

This paper reports on *WISE*-selected AGNs in the Cosmic Evolution Survey (COSMOS; Scoville et al. 2007). We use this well-studied field, which includes deep, public, panchromatic imaging from the radio to the X-ray in order to both establish *WISE* AGN selection criteria and to understand the multi-wavelength properties of *WISE*-selected AGNs. Our selection criterion identifies 130 AGN candidates in COSMOS, which is sufficient for some investigations but is too small for evolutionary studies. A companion paper, Assef et al. (2012), uses the wider area Boötes field in order to investigate the luminosity distribution and evolution of *WISE*-selected AGNs.

This paper is organized as follows. Section 2 discusses how the *WISE* and COSMOS data were matched, and motivates the simple $W1-W2 \geqslant 0.8$ criterion we use to identify AGN candidates. Section 3 describes the multiwavelength properties of *WISE*-selected AGNs, ranging from their demographics to their *Hubble Space Telescope* morphologies to their redshift distribution. As part of this investigation, we obtained Keck spectroscopy of mid-infrared selected AGN candidates in the COSMOS field, described in Section 3.7. Section 4 summarizes our results. Since COSMOS is a well-studied field, of interest to a broad segment of the astrophysical community, we include an Appendix tabulating 26 additional COSMOS sources for which we obtained spectroscopic redshifts.

Unless otherwise specified, we use Vega magnitudes throughout and adopt the concordance cosmology, $\Omega_M = 0.3$, $\Omega_\Lambda = 0.7$, and $H_0 = 70\ \mathrm{km\,s^{-1}\,Mpc^{-1}}$.

2. *WISE* SELECTION OF AGNs IN THE COSMOS FIELD

2.1. Matching *WISE* with S-COSMOS

The *Spitzer*-COSMOS survey (S-COSMOS; Sanders et al. 2007) carried out a deep (620 hr), uniform survey of the full 2 deg^2 COSMOS field in all seven *Spitzer* bands (3.6, 4.5, 5.8, 8.0, 24, 70, and 160 μm). The IRAC portion of the survey covered the field to a depth of 1200 s in the four bluest bands of *Spitzer*, with 5σ measured sensitivities ranging from 0.9 μJy at 3.6 μm to 14.6 μJy at 8.0 μm. The longer wavelength observations, obtained with the Multiband Imaging Photometer for *Spitzer* (MIPS; Rieke et al. 2004), reach 5σ sensitivities of approximately 0.07, 8.5, and 65 mJy for the 24, 70, and 160 μm arrays, respectively (Frayer et al. 2009). These depths are all considerably deeper than *WISE*.

We identified 6261 unique *WISE* sources with signal-to-noise ratio S/N $\geqslant$ 10 in *WISE* band $W2$ in a region that extends slightly beyond the FoV of the S-COSMOS survey. We used a preliminary version of the second pass data, which co-adds all observations from the *WISE* mission. In order to avoid spurious and poorly photometered sources, we limited the sample to relatively isolated sources by requiring blend flag $NB \leqslant 2$. We also avoided contaminated or confused sources by eliminating sources whose $W1$ or $W2$ photometry was affected by diffraction spikes ($ccflag = D$), persistence ($ccflag = P$), scattered light halos from nearby bright sources ($ccflag = H$), or optical ghosts ($ccflag = O$) (for a detailed description of *WISE* catalog variables, see Wright et al. 2010). The preliminary version of the second pass data we used double counts sources in the overlap regions between processing stripes.

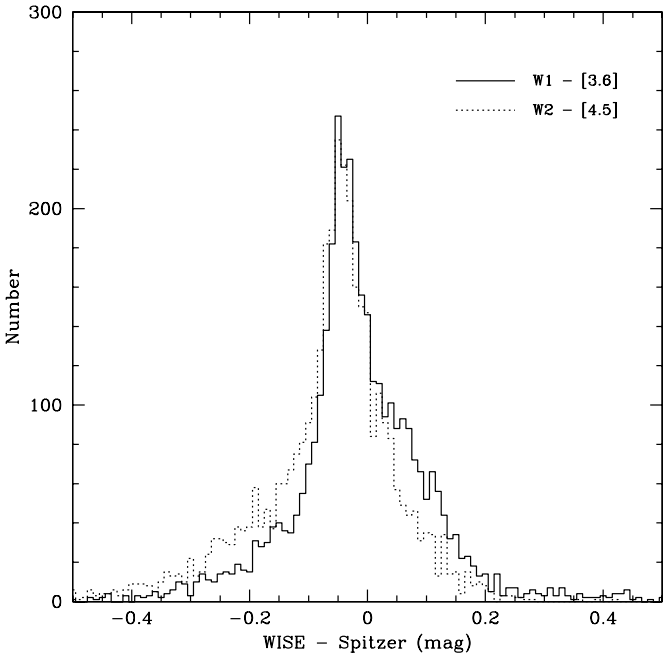

Figure 3. Distribution of offsets between *WISE* and S-COSMOS photometry for the two bluest *WISE* passbands: $W1-[3.6]$ is plotted as a solid line; $W2-[4.5]$ is plotted as a dotted line.

Using a 0.″5 match radius, we identified duplicated sources in this preliminary catalog and only retained the source with higher S/N in $W1$. The conservative (10σ) $W2$ depth we apply corresponds to an approximate flux density limit of 15.05 mag (∼160 μJy) at 4.6 μm. Most sources are also detected at $\geqslant$10σ at 3.4 μm, corresponding to 16.45 mag (∼70 μJy).

We then identified the nearest S-COSMOS source to each *WISE* source. We required detections in both IRAC channel 1 (3.6 μm) and channel 2 (4.5 μm) in order to avoid the edges of S-COSMOS, which did not receive full four-band IRAC coverage. We also eliminated saturated stars with the requirement $[3.6] \geqslant 11$. Correcting for the small mean astrometric offset between *WISE* and S-COSMOS, $\langle\Delta\mathrm{R.A.}\rangle = 0.''108$ and $\langle\Delta\mathrm{decl.}\rangle = 0.''008$, and requiring a conservative 1.″0 matching radius, we find unique, unsaturated, multi-band S-COSMOS identifications for 3618 *WISE* sources. Most of the *WISE* sources lacking S-COSMOS counterparts are from outside the S-COSMOS FoV. Within the area of good, unique matches, 4% of *WISE* sources do not have S-COSMOS counterparts and <1% of *WISE* sources have multiple S-COSMOS counterparts within the 1.″0 matching radius. Visual inspection shows that confusion is the source of both of these issues, with the lower resolution *WISE* images merging multiple objects. In the remainder of the paper, we restrict the analysis to the ∼95% of *WISE* sources within the S-COSMOS area with unique, unsaturated multi-band IRAC identifications.

Figure 3 shows the measured differences between the *WISE* and S-COSMOS photometry. For S-COSMOS, we use aperture-corrected 2.″9 photometry from the public 2007 June catalog, converted from physical units to Vega magnitudes using conversion factors prescribed by the S-COSMOS documentation available through the Infrared Science Archive (IRSA). As expected given the slightly different central wavelengths and widths of the IRAC and *WISE* filters, we find slight median offsets between their respective photometric measurements: $(W1-[3.6])_{\mathrm{med}} = -0.01$ and $(W2-[4.5])_{\mathrm{med}} = -0.07$. The Explanatory Supplement to the *WISE* All-Sky Data

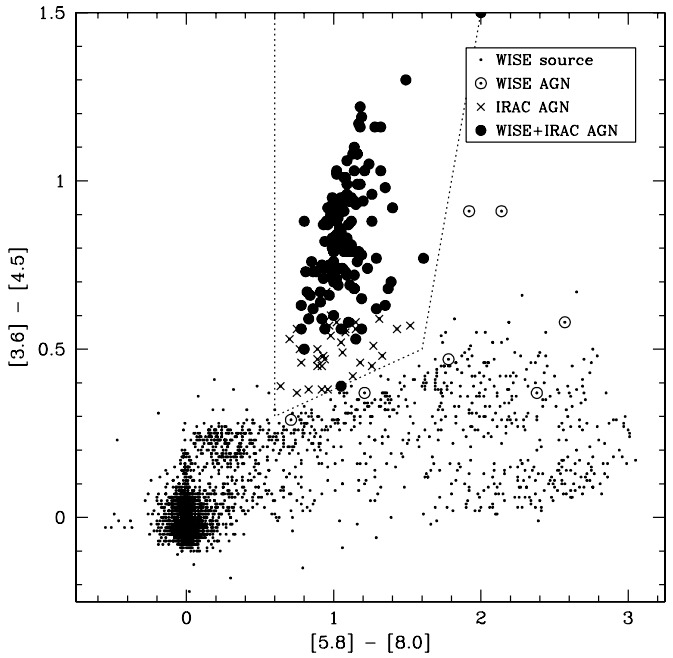

Figure 4. IRAC color–color diagram of *WISE*-selected sources in the COSMOS field. We only plot sources with S/N $\geqslant$ 10 in $W1$ and $W2$, and we require [3.6] > 11 to avoid saturated stars. Sources with $W1 - W2 \geqslant 0.8$ are indicated with larger circles; filled circles indicate sources that were also identified as AGNs using the Stern et al. (2005) mid-infrared color criteria. Sources identified as AGNs using *Spitzer* criteria but not using the *WISE* criterion are indicated with ×'s.

Release[12] finds a color term from analysis of compact sources in the *Spitzer* SWIRE *XMM*-LSS field, $(W1 - [3.6]) \sim 0.4([3.6]–[4.5])$ (see Figure 2 of Section VI.3.a of the Explanatory Supplement).

2.2. Mid-infrared Selection of AGNs with Spitzer

Figure 4 shows the IRAC color–color diagram for S-COSMOS sources with robust *WISE* counterparts. The figure shows the expected concentration of Galactic stars with Vega colors of zero. As discussed in Stern et al. (2007) and Eisenhardt et al. (2010), stars warmer than spectral class T3 all have essentially Rayleigh–Jeans continua in the IRAC passbands, leading to similar IRAC colors. Methane absorption causes redder [3.6]−[4.5] colors for cooler brown dwarfs, leading to a vertical extension above the Galactic star locus. Few such sources are found by *WISE* over an area as small as COSMOS. The sources extending to the right of the stellar locus is dominated by low-redshift star-forming galaxies, where polycyclic aromatic hydrocarbon (PAH) emission causes red [5.8]−[8.0] colors. Finally, as suggested in Eisenhardt et al. (2004) and discussed in detail in Stern et al. (2005), the vertical extension perpendicular to the galaxy sequence is dominated by AGNs. Indeed, Gorjian et al. (2008) show that the majority (65%) of X-ray sources in the XBoötes survey are identified by the Stern et al. (2005) mid-infrared criteria (see also Donley et al. 2007; Eckart et al. 2010; Assef et al. 2011). In IRAC data plotted to deeper depths, a highly populated second vertical sequence is also visible to the left of the AGN sequence. This sequence, due to massive galaxies at $z \gtrsim 1.2$ (e.g., Stern et al. 2005; Eisenhardt et al. 2008; Papovich 2008), typically outnumbers the AGN sequence since even very shallow (<90 s) IRAC pointings easily reach well below the characteristic brightness of early-type galaxies out to $z \sim 2$, $m^*_{3.6} \approx 17.5$, and $m^*_{4.5} \approx 16.7$ (e.g., Mancone et al. 2010). However, these galaxies are absent with our conservative, $W2 \lesssim 15$ magnitude cut in the much shallower *WISE* data.

In the following analysis, we will adopt the Stern et al. (2005) mid-infrared AGN sample as the "truth sample" in order to explore potential *WISE* AGN selection criteria. The Stern et al. (2005) method for selecting AGNs was one of the first methods devised to identify AGNs using *Spitzer* data and has been extensively used by other workers in the field. However, like all AGN selection criteria, it is not without some shortcomings, highlighted below.

X-ray-selected AGNs missed by mid-infrared selection. As pointed out by numerous authors (e.g., Barmby et al. 2006; Cardamone et al. 2008; Brusa et al. 2009), many X-ray sources have mid-infrared colors consistent with normal galaxies, and thus are missed by the mid-infrared AGN color criteria. As first pointed out by Donley et al. (2007) and further expanded upon by Eckart et al. (2010), the fraction of X-ray sources identified as mid-infrared AGNs increases strongly with X-ray luminosity. For example, Donley et al. (2007), using data from the Ms *Chandra* Deep Field-North (Alexander et al. 2003), find that the mid-infrared selection efficiency increases from ∼14% at $L_{0.5-8\,\mathrm{keV}} < 10^{42}\,\mathrm{erg\,s^{-1}}$ to 100% at $L_{0.5-8\,\mathrm{keV}} > 10^{44}\,\mathrm{erg\,s^{-1}}$. So while low-luminosity AGNs are, unsurprisingly, missed by the mid-infrared color selection criteria (e.g., Figures 1 and 2), such criteria appear remarkably robust at identifying the most luminous AGNs in the universe.

Contamination by star-forming galaxies. Several authors have also pointed out that the mid-infrared color cuts proposed by Lacy et al. (2004) and Stern et al. (2005) extend into regions of color space populated by star-forming galaxies (e.g., Barmby et al. 2006; Donley et al. 2008; Park et al. 2010). In order to minimize such contamination, mid-infrared power-law selection has been suggested (e.g., Alonso-Herrero et al. 2006), though Donley et al. (2012) note that systematic photometric errors from IRAC are often underestimated (e.g., Reach et al. 2005), making power-law selection more vulnerable to the quality of the mid-infrared photometry than simple color–color cuts. Donley et al. (2012) investigate contamination by star-forming galaxies using a combination of galaxy templates and real data from pure starbursts identified from *Spitzer* IRS spectroscopy. A strong conclusion from this work is that mid-infrared color selection, particularly using the Stern et al. (2005) criteria, has minimal contamination from purely star-forming galaxies below a redshift of $z \sim 1$.

Contamination by high-redshift galaxies. The Lacy et al. (2004) and Stern et al. (2005) criteria for identifying AGNs based on their mid-infrared colors were empirically derived from shallow, wide-area *Spitzer* data. In this limit, the criteria work extremely well. In deeper mid-infrared data, however, significant contamination from faint, high-redshift galaxies becomes problematic and we recommend use of the revised IRAC selection criteria of Donley et al. (2012) for deep IRAC data.

Completeness versus reliability. Finally, in choosing between the IRAC color criteria of Lacy et al. (2004) and Stern et al. (2005), we have opted for the latter. As pointed out by numerous authors (e.g., Eckart et al. 2010; Donley et al. 2012), the less selective Lacy et al. (2004) criteria have higher completeness at the cost of reliability: many more normal galaxies are identified using those criteria, yielding more significant contamination.

[12] See http://wise2.ipac.caltech.edu/docs/release/allsky/expsup/index.html.

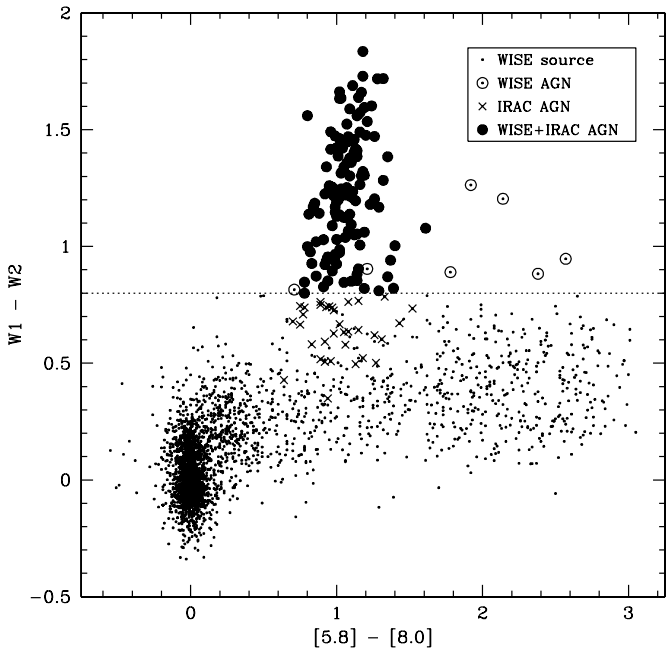

Figure 5. Mid-infrared color–color diagram of *WISE*-selected sources in the COSMOS field, with *WISE* $W1-W2$ plotted against IRAC [5.8]–[8.0]. Symbols are as in the previous figure.

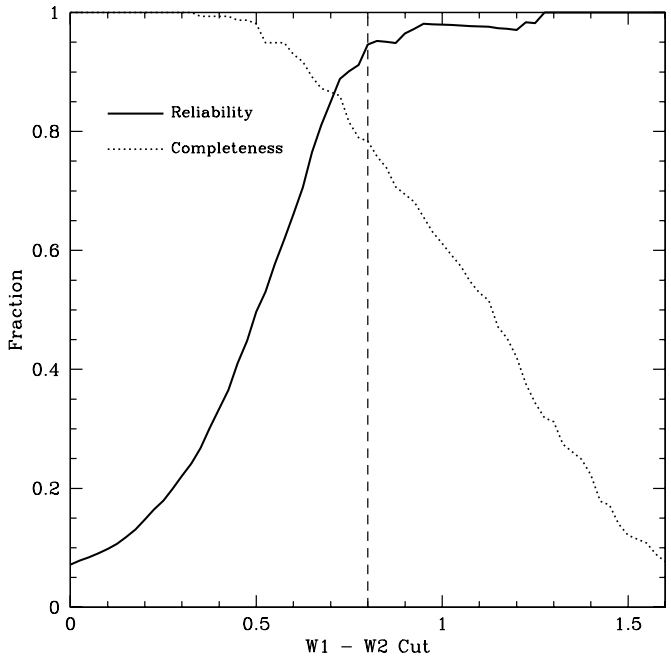

Figure 6. Reliability (solid line) and completeness (dotted line) of *WISE* AGN selection as a function of a simple $W1-W2$ color selection. Blue cuts have very high completeness, e.g., select all sources identified as mid-infrared AGN candidates according to the Stern et al. (2005) IRAC criteria. However, blue cuts have poor reliability, selecting many sources whose mid-infrared colors suggest they are normal galaxies. Likewise, red cuts robustly select AGNs with few contaminants, but have low completeness. Using the criteria $W1-W2 \geqslant 0.8$ offers both high completeness (78%) and high reliability (95%).

With the primary goal of identifying a clean sample of powerful AGNs, we therefore adopt the higher reliability IRAC color criteria of Stern et al. (2005).

In summary, we adopt the Stern et al. (2005) mid-infrared-selected AGN candidates as the "truth sample" for analyzing the *WISE* selection of AGNs. Foremost, identifying a robust truth sample identified at similar wavelength makes logical sense. Radio selection would miss ∼90% of AGNs, while optical and X-ray selection would miss the heavily obscured AGNs which are identified by mid-infrared selection but largely missed by the current generation of optical and X-ray surveys. In principle, a hybrid selection could be adopted, such as identifying all AGN candidates with $L_{\rm AGN}$ greater than some value. However, a "truth sample" identified in that manner would be vulnerable to spectroscopic incompleteness.

Despite these caveats to mid-infrared selection, we show that the Stern et al. (2005) criteria are quite robust at the shallow mid-infrared depths of *WISE*. This method identifies the most luminous X-ray-selected AGNs at high completeness. It also identifies a much higher surface density of AGNs than optical and X-ray surveys of comparable depth due to an increased sensitivity to obscured AGNs. Illustrating this point, Hickox et al. (2007) and Eckart et al. (2010) show that mid-infrared AGN candidates individually undetected at high energy are well detected in stacking analyses and reveal a harder-than-average X-ray spectrum, implying significant obscuration. Optical spectroscopy of IRAC-selected AGN candidates also typically reveal type 2 AGN spectra (D. Stern et al. 2012, in preparation). Finally, in shallow mid-infrared data, particularly at the depth of *WISE*, the Stern et al. (2005) criteria suffer from minimal contamination by Galactic stars, starburst galaxies, or high-redshift galaxies.

2.3. Mid-infrared Selection of AGNs with WISE

Figure 5 shows a hybrid mid-infrared color–color diagram. Rather than plotting IRAC [3.6]−[4.5] color along the vertical axis, we plot $W1-W2$. We see similar trends to the IRAC-only diagram (Figure 4), with a stellar locus at zero color, a horizontal sequence of low-redshift galaxies, and a vertical AGN sequence perpendicular to the galactic sequence. While mid-infrared selection of AGNs in even very shallow *Spitzer* pointings required the longer wavelength IRAC passbands to differentiate AGNs from high-redshift ($z \gtrsim 1.3$) massive galaxies, *WISE* is able to robustly identify AGNs with just $W1$ and $W2$ (e.g., see Ashby et al. 2009; Assef et al. 2010; Eckart et al. 2010). Note that these are the two most sensitive *WISE* passbands, with the highest source counts and the best spatial resolution.

We have explored how robustly *WISE* identifies AGNs using a simple $W1-W2$ color cut. Of the 3618 sources in our cross-matched *WISE*-S-COSMOS catalog, 157 are mid-infrared AGNs according to the Stern et al. (2005) criteria. We consider this the truth sample and Figure 6 shows the completeness and reliability of *WISE* AGN selection as a function of $W1-W2$ color cut. Prior to the launch of *WISE*, Ashby et al. (2009) suggested that $W1-W2 \geqslant 0.5$ would robustly identify AGNs while Assef et al. (2010) suggested a color cut of $W1-W2 \geqslant 0.85$. Considering the former, while this criterion is highly (98%) complete at identifying the AGN sample, it suffers from significant contamination from non-active sources (see Figure 6; only 50% of sources appear active according to the IRAC criteria). This is likely, in part, due to the significantly better performance of *WISE* compared to the prelaunch predictions: Mainzer et al. (2005) reported 5σ point source sensitivity requirements of 120 μJy at 3.4 μm and 160 μJy at 4.6 μm, while we are finding 10σ point source sensitivities of 70 μJy at 3.4 μm and 160 μJy at 4.6 μm. Analysis of Figure 6 suggests that a color cut at $W1-W2=0.8$ offers an extremely robust AGN sample which is still highly complete. For some uses, a slightly less

conservative color cut at $W1 - W2 = 0.7$ might be preferable, providing a powerful compromise between completeness and reliability for *WISE* AGN selection.

Using $W1 - W2 \geqslant 0.8$ to select AGN candidates, we identify 130 potential candidates, of which 123 are AGNs according to their IRAC colors (95% reliability, 78% completeness). The less conservative color cut at $W1 - W2 \geqslant 0.7$ identifies 160 candidates, of which 136 are AGNs according to their IRAC colors (85% reliability, 87% completeness), e.g., this less restrictive color cut identifies ∼10% more AGNs at the cost of tripling the number of contaminants. As seen in Figure 4, several of the "misidentified" AGN candidates have colors very close to the Stern et al. (2005) criteria. In fact, as discussed in Section 3.7, four of the seven "contaminants" for the $W1 - W2 \geqslant 0.8$ AGN selection have spectroscopic redshifts, two of which are broad-lined quasars. This implies that the above reliability numbers are likely conservative, though complete spectroscopy will be required to determine what fraction of the IRAC-selected AGNs are, in fact, not active. As seen in Figure 5, misidentified AGN candidates often have much redder [5.8]–[8.0] colors, suggestive of low-redshift galaxies with PAH emission. Potential Galactic contaminants are brown dwarfs (cooler than spectral class T1) and asymptotic giant branch stars, both of which have much lower surface densities than AGNs at the depths probed and are not expected to be a significant contaminant, particularly in extragalactic pointings.

In the following section, we use the extensive publicly available data in the COSMOS field to explore the demographics, multiwavelength properties, and redshift distribution of *WISE*-selected AGNs using the simple $W1 - W2 \geqslant 0.8$ color criterion.

3. PROPERTIES OF *WISE* AGNs

3.1. Demographics of WISE AGNs

The effective area of the S-COSMOS survey is 2.3 deg^2 per passband after removal of poor quality regions around saturated stars and the field boundary (Sanders et al. 2007). Since approximately 8% of the field is only covered by two of the four IRAC passbands, this implies a four-band effective area of approximately 2.1 deg^2. Our simple $W1 - W2$ color criterion identified 130 AGN candidates in this area, implying a surface density of 61.9 ± 5.4 *WISE*-selected AGN candidates per deg^2, up to 5% of which are expected to be T1.

For comparison, the Sloan Digital Sky Survey (SDSS) quasar selection algorithm (Richards et al. 2002) targeted ultraviolet excess quasars to $i^* = 19.1$ (AB mag; 13.0 targets per deg^2) and higher redshift ($z \gtrsim 3$) quasars to $i^* = 20.2$ (AB mag; 7.7 targets per deg^2), yielding a combined list of 18.7 candidates per deg^2. These depths are comparable to *WISE* depths for type 1 quasar selection (e.g., Assef et al. 2010). The SDSS algorithm is expected to provide over 90% completeness from simulated type 1 quasar spectra, although at the cost of lower reliability. The overall efficiency (quasars/quasar candidates) was only 66% from initial test data over 100 deg^2, with the contaminants evenly split between galaxies and Galactic stars. Importantly, optical/UV quasar selection methods are hampered at certain redshifts, especially high ones, where the stellar locus overlaps the quasar locus in color–color space. More sophisticated approaches, such as that presented in Bovy et al. (2011), work better than the old two-color or three-color cuts, though they still have issues. Other methods, such as variability (e.g., Palanque-Delabrouille et al. 2011), also do better, but require more elaborate input data sets. *WISE* selection is less affected by these problems and has a much flatter selection function as a function of redshift than traditional color-selected UV-excess methods. In particular, our simple $W1 - W2$ selection is expected to have 78% completeness and 95% reliability assuming that the Stern et al. (2005) mid-infrared selection of AGN candidates from the deeper S-COSMOS data is 100% reliable.

3.2. Mid-infrared Properties of WISE AGNs

We have studied the longer wavelength properties of *WISE*-selected AGNs with an eye toward investigating whether the inclusion of $W3$ or $W4$ would allow for a more robust *WISE* selection of AGNs, such as the wedge in $W1 - W2$ versus $W2 - W3$ color–color space presented in Jarrett et al. (2011). Our simple $W1 - W2$ color criterion identified 130 AGN candidates in COSMOS, of which 24 (18%) are detected in $W3$ ($\geqslant 10\sigma$) and only 3 (2%) are detected in $W4$ ($\geqslant 10\sigma$). If we instead use a less conservative 5σ detection threshold, we find that 78 (60%) are detected in $W3$ and 17 (13%) are detected in $W4$. These percentages are essentially unchanged when we consider the 123 robust AGN candidates identified by both the *WISE* and IRAC selection criteria: 24 (20%) are detected in $W3$ ($\geqslant 10\sigma$) and 3 (2%) are detected in $W4$ ($\geqslant 10\sigma$). Using the 5σ detection threshold, these numbers increase to 74 (60%) being detected in $W3$ and 17 (14%) being detected in $W4$.

This implies that including the longer wavelength *WISE* data increases the reliability of the AGN selection, but at the cost of a significant decrease in completeness. For example, requiring a 10σ detection in $W3$ in addition to the $W1 - W2$ color criterion provides a surface density of only 11 *WISE*-selected AGN candidates per deg^2, but the reliability is expected to be ∼100%. Using the less conservative requirement of a 5σ detection in $W3$ provides a surface density of 37 *WISE*-selected AGN candidates per deg^2 with a reliability of 95%, e.g., the same reliability as our original $W1 - W2 \geqslant 0.8$ color cut. Any of these mid-infrared selection criteria compare quite favorably with the SDSS quasar selection in terms of surface density, completeness, and reliability. However, in what follows we rely on selecting AGNs using only the single $W1 - W2 \geqslant 0.8$ color criterion, as this selection, relying on the most sensitive *WISE* passbands, identifies a much larger candidate AGN population, 2–5 times larger than the samples that also require $W3$ detections.

Finally, we note that the depth of the *WISE* survey varies strongly with ecliptic latitude. The COSMOS field was selected to be at low ecliptic latitude in order to make it accessible from both hemispheres, and thus is close to the minimum depth of the *WISE* survey with a coverage of 12 frames (11 s each). Higher latitude fields have deeper data, reaching a coverage of 250 frames at the ecliptic poles (Jarrett et al. 2011). This increases the surface density of AGN candidates, but with a decrease in robustness since deeper pointings will detect massive galaxies at $z \gtrsim 1$ which have similar $W1 - W2$ colors to AGNs. The inclusion of the deeper $W3$ data in such fields could be used to separate normal galaxies from AGNs. *WISE* selection of AGNs in deeper, higher latitude fields is addressed more thoroughly in Assef et al. (2012).

3.3. X-Ray Properties of WISE AGNs

The COSMOS field has been observed by both the *Chandra X-Ray Observatory* (Elvis et al. 2009) and *XMM-Newton* (Hasinger et al. 2007). In the following two subsections, we examine the X-ray properties of *WISE*-selected AGNs using each of these surveys.

Table 1
WISE + IRAC AGN Candidates Undetected by *Chandra*

WISE ID	i	$W1$	$W2$	$W1-W2$	[5.8]−[8.0]	z	Notes
J095855.40+022037.4	19.43	15.41	14.59	0.82	1.39	[0.38]	Bright galaxy
J095937.35+021905.9	22.30	16.00	14.70	1.30	1.17	0.927	
J100006.19+015535.3	20.90	15.53	14.19	1.34	1.05	0.661	
J100043.70+014202.5	21.77	15.89	14.89	1.00	1.40	0.741	
J100046.91+020726.5	21.86	14.87	13.14	1.73	1.18	1.158	Faint
J100135.61+022104.8	25.11	16.98	14.97	2.01	1.49	...	Faint

Note. Bracketed redshift indicates photometric redshift.

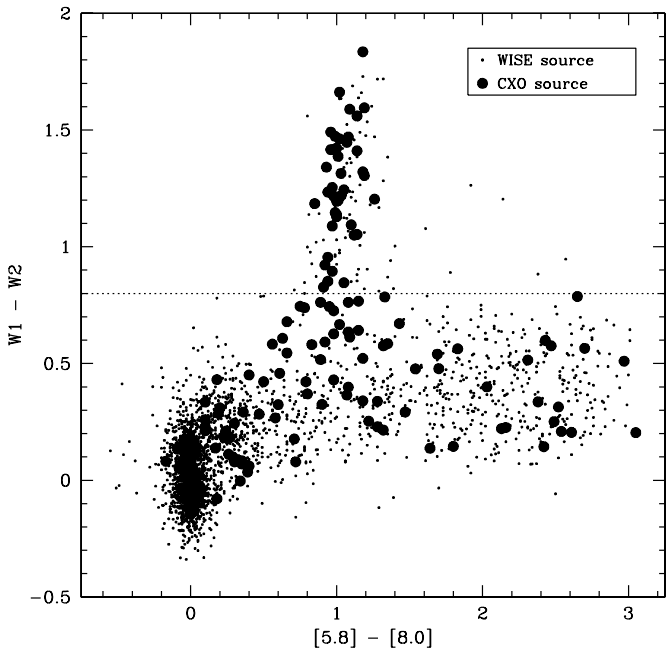

Figure 7. Mid-infrared color–color diagram of *WISE*-selected sources in the COSMOS field, with *WISE* $W1-W2$ plotted against IRAC [5.8]–[8.0]. Many of the *WISE* sources lacking *Chandra* counterparts are from outside the field of view of the C-COSMOS survey.

3.3.1. Chandra Observations

The *Chandra*-COSMOS Survey (C-COSMOS; Elvis et al. 2009) is a large, 1.8 Ms *Chandra* program that imaged the central 0.5 deg^2 of the COSMOS field with an effective exposure time of 160 ks per position and the outer 0.4 deg^2 with an effective exposure time of 80 ks per position. The corresponding point source depths in the deeper portion of the survey are 1.9×10^{-16} erg cm^{-2} s^{-1} in the soft (0.5–2 keV) band, 7.3×10^{-16} erg cm^{-2} s^{-1} in the hard (2–10 keV) band, and 5.7×10^{-16} erg cm^{-2} s^{-1} in the full (0.5–10 keV) band, where these depths assume an average X-ray power-law index $\Gamma=1.4$. C-COSMOS detected 1761 reliable X-ray point sources (catalog ver.2.1; spurious probability $<2\times10^{-5}$). We use a 2.″5 matching radius to cross-identify the *WISE* and *Chandra* sources.

A total of 167 of the *Chandra* X-ray sources have *WISE* counterparts (Figure 7). Most have relatively blue $W1-W2$ colors and are likely associated with low-redshift galaxies harboring low-luminosity AGNs; such sources are common in deep X-ray observations (e.g., Brandt & Hasinger 2005). A concentration of X-ray sources near zero mid-infrared colors are predominantly low-redshift ($z\lesssim0.6$) early-type galaxies: such galaxies have little or no star formation and therefore lack the dust and PAH emission which causes a horizontal extension in this mid-infrared color–color space. Finally, deep *Chandra* surveys are also sensitive to X-ray emission from low-mass Galactic stars, which likewise reside in this same region of color–color space (e.g., Stern et al. 2002b).

More interesting is the vertical extension seen in Figure 7: 41 of the *WISE*-selected AGN candidates have C-COSMOS counterparts. Most of the *WISE* + IRAC AGN candidates lacking *Chandra* counterparts in Figure 7 are from outside the C-COSMOS FoV. Six (e.g., 13%) of the *WISE*-selected AGN candidates whose IRAC colors are consistent with the Stern et al. (2005) AGN selection criteria were observed by, but *not* detected by *Chandra*. We list these sources in Table 1. All are at least 9″ from the nearest *Chandra* source. These mid-infrared sources are strong candidates for Compton-thick AGNs (e.g., $N_{\rm H}\geqslant10^{24}$ cm^{-2}): sources with so much internal absorption that their X-ray emission below 10 keV is heavily absorbed, undetected in the ∼100 ks *Chandra* observations. The absorbing material, however, is heated up and is easily detected in ∼100 s integrations with *WISE*. We also note, as expected, that the small number of *WISE* AGN contaminants with $W1-W2\geqslant0.8$ but whose IRAC colors are *not* consistent with an AGN are undetected by *Chandra*.

Figure 8 shows the relationship between hard X-ray (2–10 keV) fluxes of S-COSMOS sources and their hardness ratios HR $\equiv(H-S)/(H+S)$, where H and S are the numbers of hard and soft X-ray photons detected, respectively. We compare the full sample (smallest black dots) to the subset with *WISE* counterparts (small black circles) to the smaller set of sources with IRAC and/or *WISE* colors indicative of AGN activity (larger symbols). Note that many of the brightest X-ray sources in the field are identified as AGN candidates by *WISE*, regardless of their hardness ratio.

3.3.2. XMM-Newton Observations

The *XMM-Newton* wide-field survey of the COSMOS field (*XMM*-COSMOS; Hasinger et al. 2007; Brusa et al. 2010) observed the entire 2 deg^2 COSMOS field to medium depth (∼60 ks). The survey detected nearly 2000 X-ray sources down to limiting fluxes of $\sim5\times10^{-16}$ erg cm^{-2} s^{-1} in the 0.5–2 keV (soft) band and $\sim3\times10^{-15}$ erg cm^{-2} s^{-1} in the 2–10 keV (hard) band. Thus, *XMM*-COSMOS covers a wider area than C-COSMOS, albeit to shallower depth. We use the 2008 November *XMM-Newton* point-like source catalog, available thru IRSA, which contains 1887 sources. Using a 3.″5 matching radius—slightly larger than used for C-COSMOS to account for the poorer spatial resolution of *XMM-Newton*—we identify *WISE* counterparts for 244 *XMM*-COSMOS sources, of which 92 have $W1-W2\geqslant0.8$. The mid-infrared color distribution of *XMM* sources is similar to what was seen for C-COSMOS, though more of the mid-infrared AGN candidates

Table 2
WISE + IRAC AGN Candidates Undetected by *XMM-Newton*

WISE ID	i	$W1$	$W2$	$W1-W2$	[5.8]−[8.0]	z	Notes
J095733.79+020943.1	19.66	16.33	15.08	1.25	1.07	1.441	SDSS QSO
J095736.56+020236.7	21.31	16.12	14.74	1.38	1.35	...	
J095752.32+022021.2	18.80	15.75	14.47	1.28	1.32	2.050	SDSS QSO
J095756.65+020719.5	20.27	15.67	14.87	0.80	0.78	[0.31]	
J095821.40+025259.0	19.53	15.67	14.50	1.17	1.29	...	
J095855.40+022037.4	19.43	15.41	14.59	0.82	1.39	[0.38]	Bright galaxy
J095905.55+025145.0	19.85	15.95	15.08	0.87	1.35	...	
J095937.35+021905.9	22.30	16.00	14.70	1.30	1.17	0.927	
J095945.60+013032.2	20.34	15.97	15.01	0.97	0.99	1.106	SDSS QSO
J100006.19+015535.3	20.90	15.53	14.19	1.34	1.05	0.661	
J100008.42+020247.4	20.24	15.87	14.82	1.05	1.12	0.370	Type-2 AGN
J100008.93+021440.5	18.93	15.93	14.72	1.20	1.26	2.536	QSO
J100013.51+013739.2	19.94	16.23	14.83	1.40	1.12	1.608	SDSS QSO
J100043.70+014202.5	21.77	15.89	14.89	1.00	1.40	0.741	
J100046.91+020726.5	21.86	14.87	13.14	1.73	1.18	1.158	Faint
J100115.38+024231.4	20.44	16.21	15.02	1.20	1.13	...	
J100135.61+022104.8	25.11	16.98	14.97	2.01	1.49	...	Faint
J100137.11+024650.6	21.58	16.36	14.87	1.49	1.16	0.143	
J100142.22+024330.7	22.69	15.74	14.02	1.72	1.28	[1.62]	
J100231.86+015242.3	21.01	15.85	14.68	1.17	0.99	...	
J100244.77+025651.5	20.26	15.86	14.72	1.14	1.09	...	
J100246.35+024609.6	19.08	15.63	14.69	0.94	1.37	...	
J100253.31+020222.1	20.84	15.32	14.24	1.08	1.61	0.902	
J100303.46+022632.0	20.69	15.68	14.82	0.85	1.14	...	
J100305.98+015704.0	19.46	14.63	12.91	1.72	1.32	0.370	Type-2 AGN
J100322.00+014356.5	...	16.21	15.08	1.12	1.05	...	

Note. Bracketed redshifts indicate photometric redshifts.

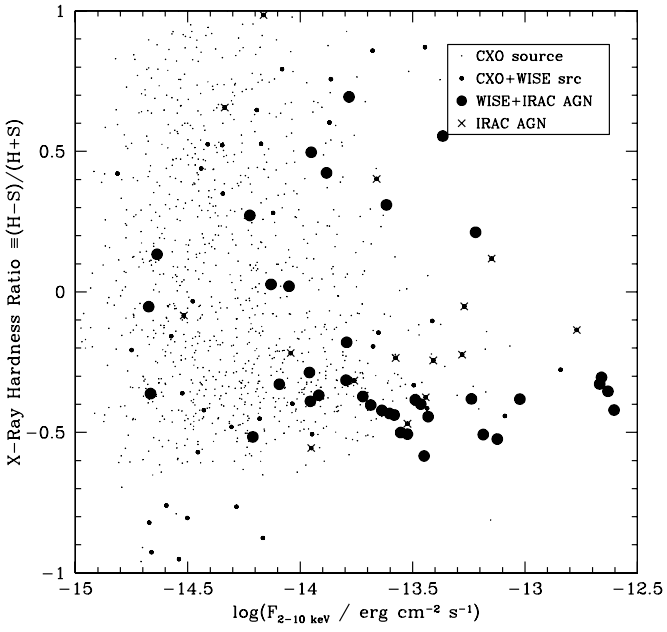

Figure 8. X-ray hardness ratio HR $\equiv (H-S)/(H+S)$, where H (S) is the number of detected hard (soft) X-ray counts, plotted against hard X-ray flux. All X-ray data are from *Chandra*; at the depth of these data, most X-ray sources are expected to be AGNs. We identify no *Chandra* counterparts for the *WISE*-selected AGN candidates whose IRAC colors are indicative of being normal, non-active galaxies. Note that many (but not all) of the brightest hard X-ray sources are identified as AGN candidates by both *WISE* and IRAC.

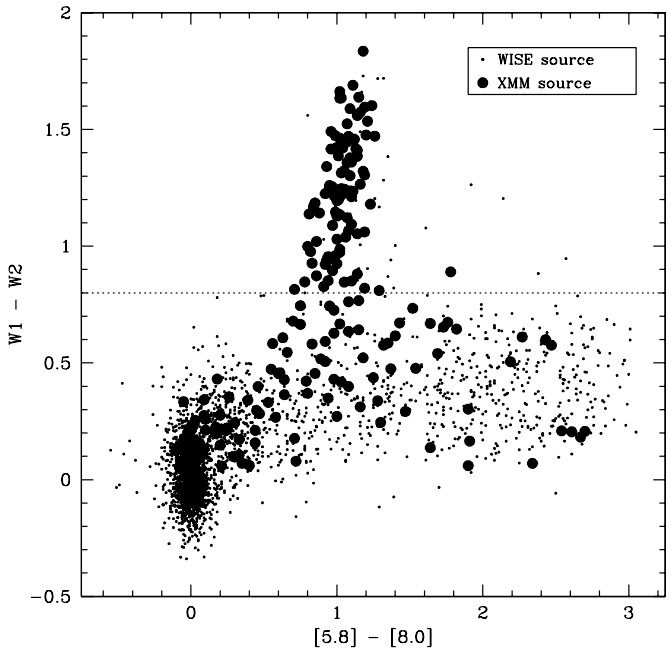

Figure 9. Mid-infrared color–color diagram of *WISE*-selected sources in the COSMOS field, with *WISE* $W1-W2$ plotted against IRAC [5.8]–[8.0]. Dots show all *WISE* sources in the field, larger filled circles show *WISE* sources with *XMM* counterparts.

have X-ray detections courtesy of the wider spatial coverage of this survey (Figure 9). Thirty-three *WISE* sources whose IRAC colors suggest an active nucleus (out of 123) are undetected by *XMM-Newton*, though seven are from outside the *XMM-Newton* coverage; the other 26 are listed in Table 2. All six of the sources from Table 1 remain undetected by *XMM-Newton*.

Therefore, 75% of the *WISE*-selected AGN candidates have *XMM-Newton* counterparts, but that still leaves a significant number of *WISE*-selected AGNs—including those whose IRAC colors indicate an AGN—that are *undetected* by *XMM-Newton*.

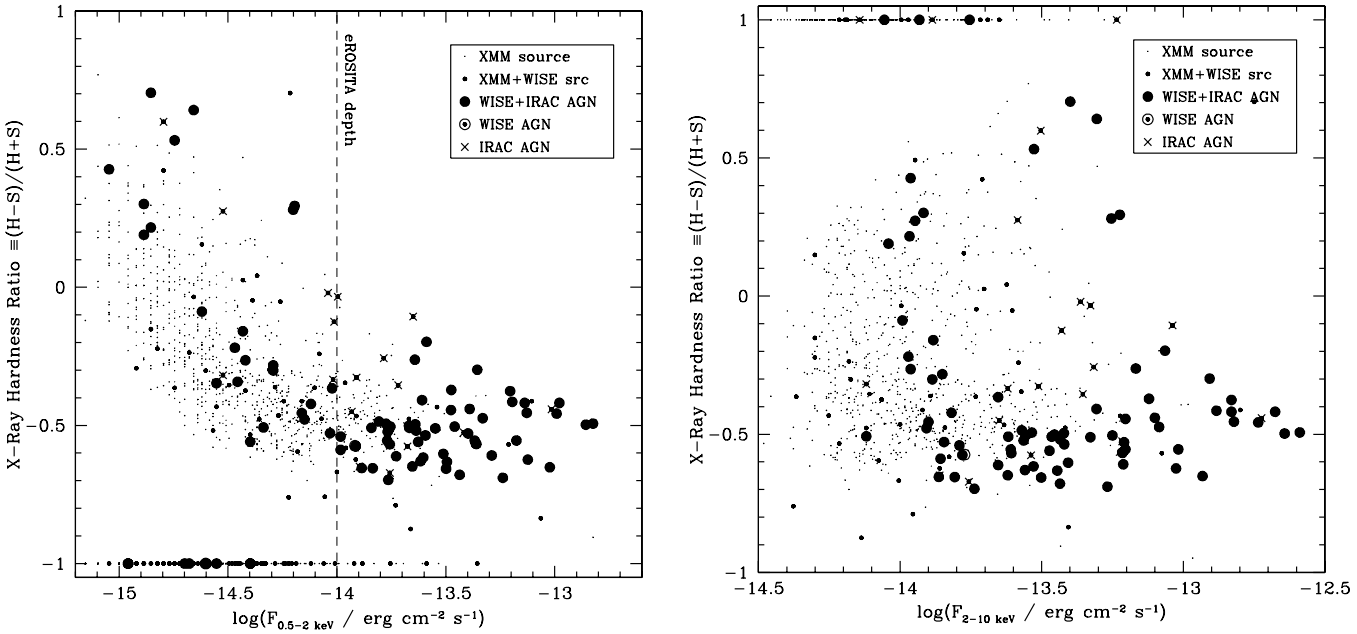

Figure 10. X-ray hardness ratio HR from *XMM-Newton* plotted against X-ray flux (right: soft-band, 0.5–2 keV; left: hard-band, 2–10 keV). Note that many (but not all) of the brightest hard X-ray sources are identified as AGN candidates by both the *WISE* criterion and by their IRAC colors (large black circles). The vertical dashed line in the left panel shows the expected soft-band point source sensitivity of the all-sky eROSITA survey; the hard-band point source sensitivity corresponds approximately to the right-hand axis of the high-energy panel. While the brightest soft X-ray sources are expected to also be identified by eROSITA, many *WISE*-selected AGN candidates are below the eROSITA flux limits. Conversely, eROSITA is expected to identify many lower luminosity AGNs that are not identified as AGN candidates by *WISE*.

We also note that two of the sources with $W1-W2 \geqslant 0.8$ but outside of the Stern et al. (2005) IRAC wedge are detected in the X-rays; both have IRAC colors very close to the wedge defined in that paper.

Similar to the *Chandra* results, we find that the *WISE*-selected AGNs are brighter and have softer spectra than typical *XMM-Newton* sources in *XMM*-COSMOS. However, Figure 10 also shows quite clearly that the brightest X-ray sources tend to be identified as AGN candidates from their *WISE* colors, regardless of X-ray hardness ratio. For comparison, we also plot the expected point source sensitivity of the all-sky eROSITA telescope. The brightest soft X-ray sources, $F_{0.5-2\,\mathrm{keV}} \gtrsim 2\times10^{-14}\,\mathrm{erg\,cm^{-2}\,s^{-1}}$, will basically all already have been identified as AGN candidates by *WISE*. At the sensitivity limit of eROSITA, however, large numbers of X-ray sources are expected that are not identified by *WISE*; these are likely lower luminosity AGNs at lower redshifts (e.g., Eckart et al. 2010; Donley et al. 2012). *WISE* also detects a significant population of fainter, harder spectrum X-ray sources, below the sensitivity limit of eROSITA. These results, particularly Figure 10, emphasize the complementarity of X-ray and mid-infrared AGN selection: each selection technique identifies samples of AGNs missed by the other technique.

Finally, using the greater statistics of the *XMM-Newton* sample, we consider if there are any trends between X-ray hardness ratio and mid-infrared $W1-W2$ color. Though no strong correlation is evident, we do find the expected general trend of redder mid-infrared sources having harder X-ray spectra. Splitting the X-ray sample at HR = 0, the softer mid-infrared AGN candidates (e.g., $HR < 0$) have a mean *WISE* color of $\langle W1-W2\rangle = 1.18$. In contrast, the harder mid-infrared AGN candidates (e.g., HR > 0) have a mean *WISE* color of $\langle W1-W2\rangle = 1.32$. However, there are examples of very hard X-ray sources with relatively blue *WISE* colors, as well as very soft X-ray sources with relatively red *WISE* colors.

3.4. Radio Properties of WISE AGNs

The Very Large Array (VLA) obtained deep radio images of the COSMOS field at 20 cm. The goals, observing strategy, and data reductions for this large program, called the VLA-COSMOS survey, are described in Schinnerer et al. (2007). The survey entailed nearly 350 hr of exposure time, primarily in the highest resolution, or A, configuration. The Large project imaged the full 2 deg^2 COSMOS field with a resolution of 1.″5 to a sensitivity of $\sim$11 μJy (1σ) (Bondi et al. 2008). We use the joint catalog of Schinnerer et al. (2010), which combines an improved analysis of the Large project with data from the Deep project that doubled the integration time in the central 0.84 deg^2 region of the survey. The Joint catalog includes 2865 sources, of which 131 consist of multiple components.

We match the full Joint catalog to the full *WISE* source list of 3618 sources using a 1.″5 matching radius. We find 333 matches, of which 33 have multiple components in the VLA data. Figure 11 shows the mid-infrared colors of the VLA sources, which shows many radio-detected sources on both sides of our $W1-W2=0.8$ color cut. This is unsurprising, as these extremely deep radio data detect emission related to stellar processes (e.g., supernova remnants) as well as AGN activity at a range of Eddington ratios. Considering the *WISE*-selected AGN candidates, 55 of the 130 candidates (42%) have radio matches; five of these are flagged as consisting of multiple components in the radio data. Of the 123 AGN candidates identified by both *WISE* and IRAC, 52 (42%) are detected by these very deep radio data. For the *WISE*-selected AGNs not flagged as likely AGNs by IRAC, three (43%) are detected by the VLA. All of these fractions are much higher than the 8% of sources with $W1-W2<0.8$ which are detected by the VLA-COSMOS survey.

Assuming a typical quasar radio spectral index $\alpha = -0.5$ ($S_\nu \propto \nu^\alpha$) and adopting the Gregg et al. (1996)

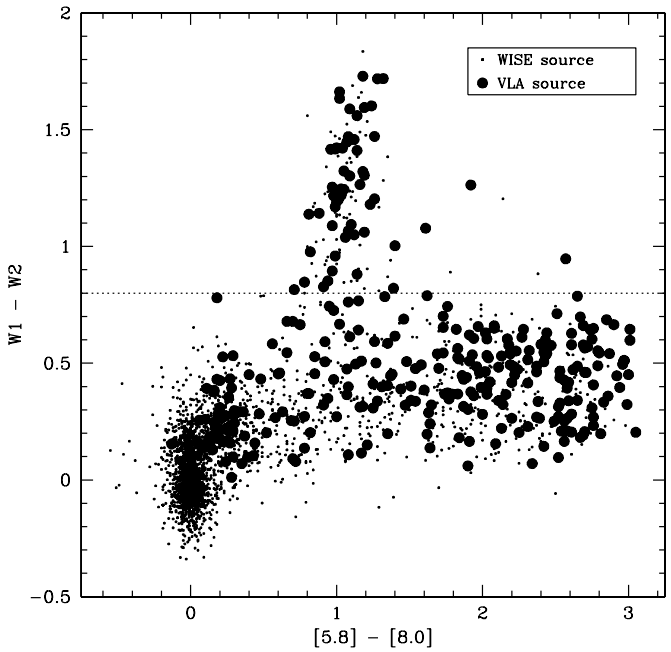

Figure 11. Mid-infrared color–color diagram of *WISE*-selected sources in the COSMOS field, with *WISE* $W1-W2$ plotted against IRAC $[5.8]-[8.0]$. Plotted sources and symbols are as in Figure 5, with large black circles added for all *WISE* sources with VLA counterparts in the VLA-COSMOS survey.

cutoff value for the 1.4 GHz specific luminosity, $L_{1.4\,\mathrm{GHz}} = 10^{32.5}\,h_{50}^{-2}\,\mathrm{erg\,s^{-1}\,Hz^{-1}}$ ($\approx 10^{24}\,h_{50}^{-2}\,\mathrm{W\,Hz^{-1}\,sr^{-1}}$), to discriminate radio-loud and AGN radio-quiet populations, only 2 of the 98 *WISE*-selected AGNs with spectroscopic redshifts are radio loud.[13] The results are unchanged if we assume $\alpha = -0.8$, as might be more typical for quasars without the jet aligned along our line of sight. Both of these sources are SDSS quasars at $z > 1$ (WISE J095821.65+024628.2 at $z = 1.405$ and WISE J095908.32+024309.6 at $z = 1.318$). These two sources come from a total of 45 *WISE*-selected AGNs that are optically bright and have spectroscopy from the SDSS; all are classified as broad lined, and 35 are at $z > 1$, implying that they are clearly luminous quasars. Considering just this SDSS subsample of *WISE*-selected AGNs, our results are statistically consistent with the canonical value of ∼10% of quasars being radio loud (e.g., Stern et al. 2000b). However, the fact that none of the 53 other sources with spectroscopic redshifts are radio loud is surprising, suggesting that the radio-loud fraction might be different for type 2 AGNs. We note, however, that Zakamska et al. (2004) found no change in the radio-loud fraction for their sample of SDSS-selected obscured quasars.

Note that radio-loud AGNs do not fall below the 5σ VLA-COSMOS sensitivity until beyond $z \sim 10$, e.g., the survey is sensitive enough to detect all radio-loud AGNs that *WISE* is likely to detect. All of the *WISE*-selected AGN candidates without redshifts that were detected by the VLA-COSMOS survey have $S_\nu < 0.72$ mJy, implying that they would have to be at $z > 3.4$ in order to be radio loud.

3.5. Optical Magnitudes and Colors of WISE AGNs

We next consider the optical properties of the *WISE*-selected AGN candidates. Figure 12 shows the *r*-band magnitude distributions of all *WISE* sources in the COSMOS field (open histogram) as well as the AGN candidates with $W1 - W2 \geqslant 0.8$ (solid histogram). All photometry is in the AB system and comes from the COSMOS photometry catalog of Capak et al. (2007), which is available through IRSA. The left panel shows *r*-band photometry from the second data release (DR2) of the SDSS (Abazajian et al. 2004). Objects as bright as 10th mag have good photometry in the SDSS imaging, and the imaging depth, defined as the 95% completeness limit for point sources, is $r \sim 22.2$. Similar data are available over more than 11,000 deg^2. However, many of the *WISE* sources are fainter than this limiting depth, so in the right panel of Figure 12 we show the Subaru r^+ photometry in the COSMOS field obtained with the Suprime-Cam instrument (Komiyama et al. 2003). These data reach a 5σ depth ($3''$ aperture) of 26.6 and detect all of the *WISE*-selected

[13] For consistency with previous work in terms of defining the boundary between radio-loud and radio-quiet populations, 1.4 GHz specific luminosity is calculated for an Einstein–de Sitter cosmology, e.g., see Stern et al. (2000b).

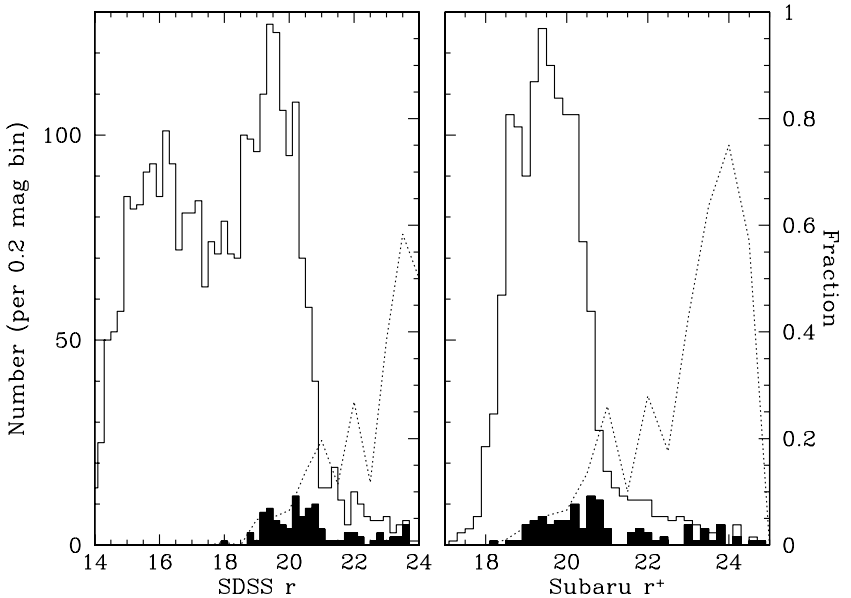

Figure 12. Histograms of SDSS *r*-band (left) and Subaru r^+-band (right) optical magnitudes of all *WISE*-selected sources in the COSMOS field (open histogram). Solid histograms show distributions for *WISE*-selected AGN candidates. Dotted lines show the fraction of *WISE* sources that are AGN candidates as a function of optical magnitude (in 0.5 mag bins). While very few sources brighter than ∼19th mag are AGN candidates, the fraction increases to >50% at the faintest magnitudes.

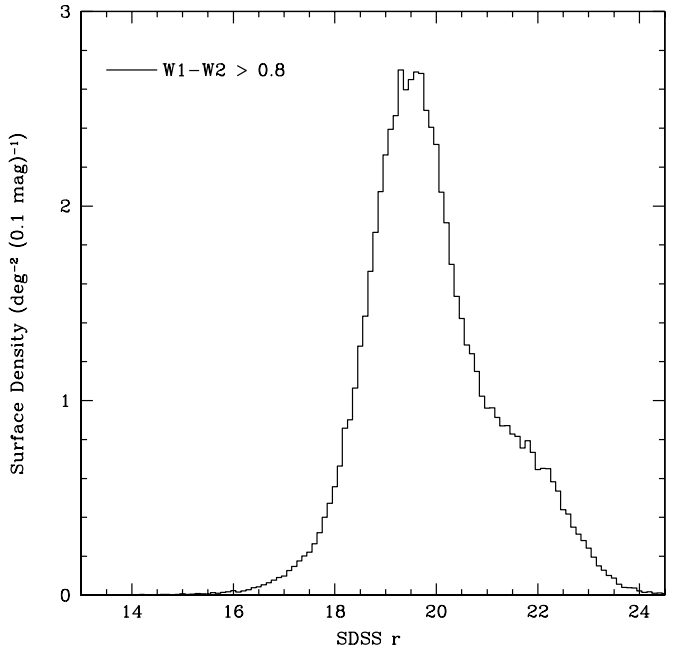

Figure 13. Distribution of *r*-band magnitudes for *WISE*-selected AGN candidates identified over 4000 deg^2 of the SDSS.

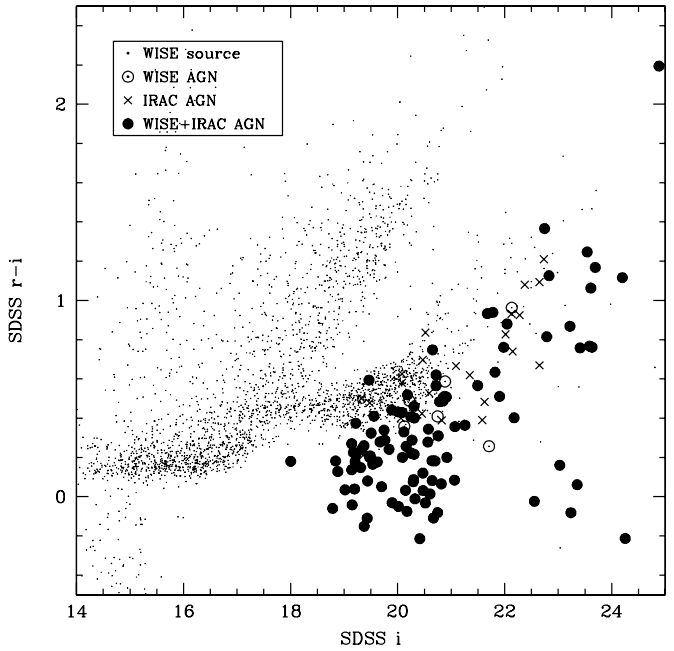

Figure 14. Optical color–magnitude diagram of *WISE* sources in the COSMOS field. Optical photometry is from SDSS, and symbols are indicated in the upper left. *WISE*-selected AGN candidates tend to optical colors that are bluer than typical field sources, though a significant fraction of the AGN candidates overlap with the field population.

AGN candidates. Many of the brighter sources in the Subaru data are unresolved, leading to saturation issues. This causes the truncation seen at $r^+ \lesssim 18$.

Figure 12 shows that very few of the *WISE*-selected AGN candidates are brighter than $r \sim 18$, and they represent less than 5% of the *WISE* source population at bright optical magnitudes. However, the AGN candidates represent an increasing fraction of the optically fainter *WISE* sources, accounting for ∼20% of *WISE* sources at $r \sim 21$ and more than 50% of *WISE* sources with $r \gtrsim 23$. In order to explore the optical brightnesses of *WISE*-selected AGN candidates with higher fidelity, we identified AGN candidates over 4000 deg^2 of the SDSS (cf., Donoso et al. 2012; Yan et al. 2012). Figure 13 shows the resultant *r*-band distribution. While the majority of AGN candidates are well detected in the SDSS imaging, their optical brightness distribution peaks at $r \sim 19.5$, making them fainter than the typical spectroscopic limits of SDSS, $i \sim 19.1$ for quasars and $r \sim 17.8$ for galaxies (as discussed in the following section, approximately half of our *WISE*-selected AGN candidates are spatially resolved).

Figure 14 shows an optical color–magnitude diagram of *WISE* sources. At bright magnitudes, the distribution is dominated by Galactic stars with $r - i \sim 0.1$, while a second galaxy sequence becomes evident at $r \gtrsim 18$. Mid-infrared AGN candidates are, on average, bluer than typical galaxies, though the color distribution clearly overlaps with the galaxy sample. AGN candidates identified by both *WISE* and *Spitzer*/IRAC, which represent the most robust AGN sample with the highest rate of X-ray detections, tend to be bluer than galaxies at $i \lesssim 21$, though at fainter magnitudes where obscured AGNs become more prevalent, the distribution fans out. This is partially due to photometric errors, but also because a large fraction of the AGN candidates have colors similar to galaxies. Not surprisingly, AGN candidates identified by *Spitzer* but not by *WISE*—e.g., sources at the blue corner of the Stern et al. (2005) wedge and close to the galaxy locus in mid-infrared color–color space—tend to have galaxy-like optical colors.

3.6. Morphologies of WISE AGNs

Conventional wisdom states that the most luminous AGNs in the universe are associated with unresolved point sources at optical wavelengths. While this is true for the vast majority of unobscured, type 1 quasars, this is not the case for obscured, type 2 quasars. For instance, luminous high-redshift radio galaxies often have a clumpy, irregular morphology at rest-frame ultraviolet wavelengths, with the emission generally elongated and aligned with the radio source axis (e.g., McCarthy et al. 1987). At rest-frame optical wavelengths, where stars dominate the galaxy luminosity, the hosts of most luminous radio galaxies are normal elliptical galaxies with $r^{1/4}$-law light profiles (e.g., Zirm et al. 2003).

The cornerstone data set for the COSMOS survey is its wide-field *Hubble Space Telescope* Advanced Camera for Surveys (ACS) imaging (Scoville et al. 2007; Koekemoer et al. 2007). With 583 single-orbit F814W (I_{814} hereafter) observations, these data cover (or define) the 1.8 deg^2 COSMOS field and constitute the largest contiguous *Hubble* imaging survey to date. The data are extremely sensitive, with 0.″09 resolution (FWHM) and reaching a 50% completeness limit of $I_{814} = 26.0$ (AB) for sources 0.″5 in diameter.

Griffith & Stern (2010) have recently analyzed the optical morphologies of AGNs in the COSMOS field identified from a variety of methods: radio selection, X-ray selection, and mid-infrared selection (see also Gabor et al. 2009). They find that the radio-selected AGNs are likely to be hosted by early-type galaxies, while X-ray- and mid-infrared-selected AGNs are more often associated with point sources and disk galaxies. Considering just the brighter X-ray and mid-infrared subsamples, approximately half of the AGNs are optically unresolved and a third are associated with disk galaxies. These morphological results conform with the results of Hickox et al. (2009) who studied the colors and large-scale clustering

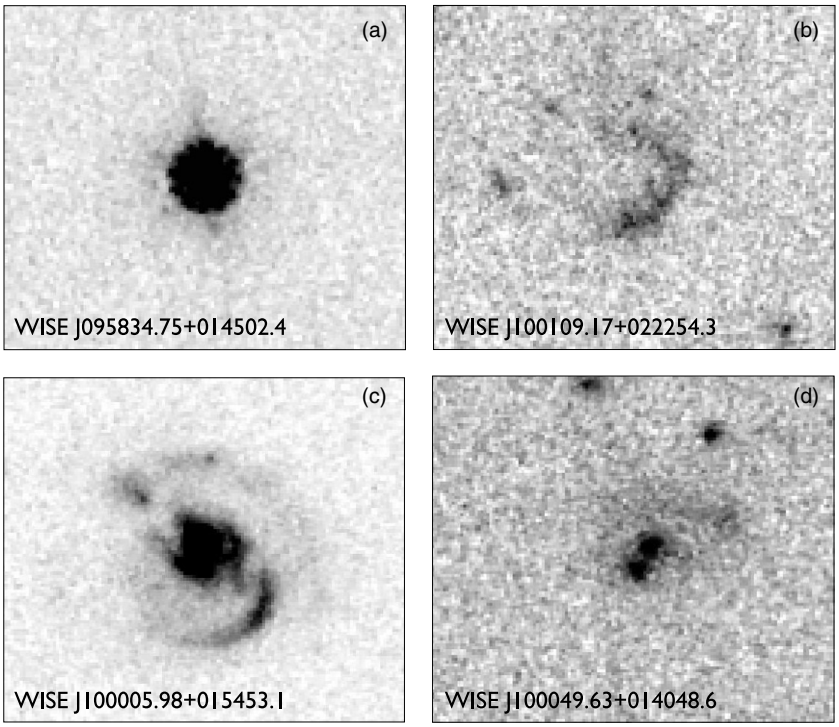

Figure 15. *Hubble*/ACS I_{814} images of four *WISE*-selected AGN in the COSMOS field, showing the range of optical morphologies. Approximately half of the sources are unresolved point sources (e.g., panel (a)). The other half are spatially resolved (e.g., panels (b)–(d)), sometimes with rather faint optical magnitudes. All four sources shown here are identified as candidate AGNs by both *WISE* and IRAC color criteria. Images are ∼4″ on a side (e.g., smaller than the *WISE* PSF), with north up and east to the left.

of AGNs, and found a general association of radio-selected AGNs with "red sequence" galaxies (an old, well-known result; e.g., Matthews et al. 1964), mid-infrared-selected AGNs are associated with "blue cloud" galaxies, and X-ray-selected AGNs straddle these samples in the "green valley."

We find similar results here. Of the 130 *WISE*-selected AGN candidates, 94 are located within the portion of COSMOS imaged by ACS. A bit more than half (52/94, or 55%) of the sources are spatially resolved; the other AGN candidates are associated with point sources. As an aside, we note that one of the contaminants, WISE J100050.63+024901.7, was flagged by Faure et al. (2008) as one of the 20 most likely strong lensing systems in the COSMOS field (see also Jackson 2008). The ACS I_{814} image of this system shows four faint arcs surrounding a bright early-type galaxy, with a radial separation of 1.″9. Inspection of the IRAC images for this system shows that the mid-infrared data are still dominated by the optically bright lensing galaxy.

Figure 15 shows *Hubble*/ACS I_{814} images of four example *WISE*-selected AGNs. All four examples were also identified as AGN candidates by their IRAC colors. Several are X-ray and/or radio sources as well. Panel (a) shows WISE J095834.75+014502.4, a bright SDSS quasar at $z = 1.889$. It is unresolved in the ACS image; approximately half of the *WISE* AGN candidates have similar morphologies. Panel (b) shows WISE J100109.21+022254.2, one of the optically faintest *WISE*-selected AGN candidates in the COSMOS field, with $I_{814} = 22.9$. As discussed in the next section, we were unable to obtain a redshift for this source from deep Keck spectroscopy, though subsequent to our observations, Brusa et al. (2010) reported that this source is as a narrow-lined AGN at $z = 1.582$. Panels (c) and (d) show two $z \sim 0.9$ type 2 (e.g., narrow-lined) AGNs from Trump et al. (2007). The former is WISE J100005.99+015453.3, which is a spiral galaxy with a very bright nucleus. The latter is WISE J100013.42+021400.4, which has a more irregular morphology.

Figure 16 presents a color–magnitude diagram of *WISE* sources in the COSMOS field, with optical-to-mid-infrared color plotted against 4.6 μm brightness ($W2$). For the AGN candidates, we only plot the ∼70% of sources covered by the ACS imaging. There are several things to note from this plot. First, the *WISE*-only AGN candidates (e.g., *WISE*-selected AGN candidates not identified as AGN candidates from their *Spitzer* colors) clearly reside on the right side of Figure 16, with no contaminants brighter than $W2 = 14.8$. This implies that caution should be applied before extending our simple *WISE* color criterion to fainter limits. Indeed, in Assef et al. (2012) we investigate the interloper fraction as a function of $W2$ magnitude and derive a magnitude-dependent *WISE* AGN selection criterion applicable to higher ecliptic latitude (e.g., deeper) portions of the *WISE* survey.

Second, optically unresolved AGN candidates tend to have bluer $r - W2$ colors, consistent with the expectation that they suffer less extinction at optical wavelengths. Quantitatively, the unresolved *WISE*+IRAC AGN candidates in Figure 16 have $\langle r - W2 \rangle = 5.18$. Similarly selected sources that are resolved in the *Hubble* imaging have $\langle r - W2 \rangle = 7.29$. The unresolved AGN candidates are also slightly brighter, with $\langle W2 \rangle = 14.54$ as compared to $\langle W2 \rangle = 14.69$ for the resolved *WISE*+IRAC AGN candidates. Importantly, however, we note that both resolved and unresolved sources are found across the full $W2$ range probed.

Finally, we also consider the optical properties of the *WISE*+IRAC AGN candidates that are undetected by *XMM-Newton* (Table 2). These sources have an even fainter median mid-IR brightness, $\langle W2 \rangle = 14.72$, and also have redder optical-to-mid-IR colors than typical *WISE*+IRAC AGN candidates.

Table 3
Results of 2010 March Keck Observations

I_{814}	R.A.	Decl.	z	Slitmask(s)	Notes
20.52	10:00:14.09	+02:28:38.5	1.2591	D[6]	QSO: Mg II, [O II], [Ne III]
20.47	10:00:36.06	+02:28:30.5	0.6883	D[5]	[O II], Hβ, [O III]
22.91	10:01:09.23	+02:22:54.5		B, D[2]	Faint blue cont.; $z = 1.582$ in Brusa et al. (2010)
19.16	10:01:14.29	+02:23:56.8	1.7997	B, D[1]	QSO: Lyα, C IV, C III], Mg II
20.04	10:01:18.58	+02:27:39.1	1.0420	B	QSO: C IV, C III], Mg II, [Ne V], [O II], [Ne III]
18.85	10:02:32.13	+02:35:37.3	0.6568	A	QSO: Mg II, [Ne IV], [O II]; jet?
19.30	10:00:22.79	+02:25:30.6	0.3482	D[3]	Hα

Notes. Masks A and B were observed with LRIS. Mask D was observed with DEIMOS; the bracketed numbers indicate the DEIMOS slitlet number. All derived redshifts are of very high quality (Q = A; see the Appendix).

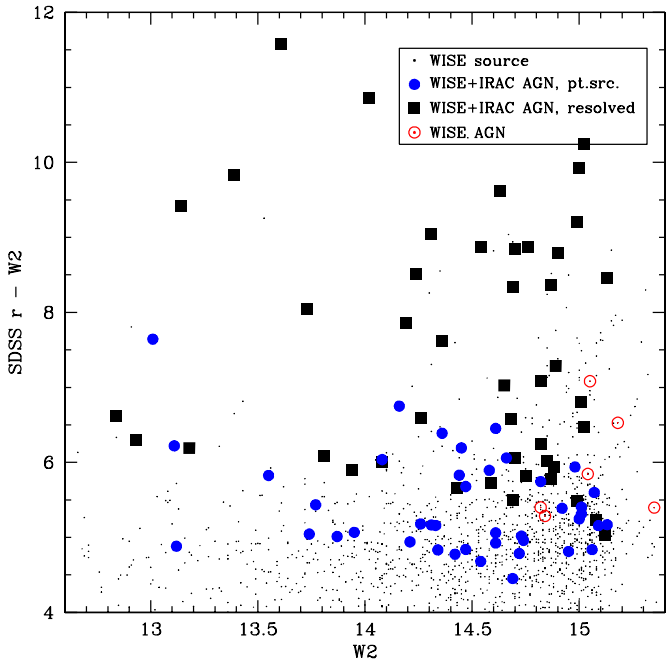

Figure 16. Optical-to-mid-infrared vs. mid-infrared color–magnitude diagram of *WISE*-selected sources in the COSMOS field. Optical photometry is from SDSS, and symbols are indicated in the upper left. Only those AGN candidates covered by the COSMOS *Hubble* images are plotted, and they are flagged by their ACS morphologies.

(A color version of this figure is available in the online journal.)

Quantitatively, $\langle r - W2 \rangle = 6.58$ for the X-ray-undetected AGN candidates, while $\langle r - W2 \rangle = 5.85$ for the X-ray-detected *WISE*+IRAC AGN sample. This is consistent with the X-ray-undetected sources being associated with more heavily obscured AGNs, diminishing both their optical and X-ray fluxes.

3.7. Redshift Distribution of WISE AGNs

In order to understand the redshift distribution and properties of *WISE*-selected AGN candidates, we have both matched the candidate list to publicly available spectroscopy in the COSMOS field and obtained new observations. Published spectroscopy come from several papers: bright targets have spectroscopic redshifts from the SDSS (Abazajian et al. 2009); Prescott et al. (2006) report on MMT/Hectospec follow-up of optically selected quasar candidates in COSMOS; Lilly et al. (2007) report on *z*COSMOS, a large VLT/VIMOS *I*-band magnitude-limited survey of the COSMOS field; Trump et al. (2007) and Trump et al. (2009) report on Magellan/IMACS spectroscopy of X-ray- and radio-selected AGN candidates in the COSMOS field; and Brusa et al. (2010) report on spectroscopy of X-ray sources from the *XMM-Newton* wide-field survey of the COSMOS field, synthesizing both previously published results and new spectroscopy from Keck.

We obtained additional spectroscopy on UT 2010 March 12–15 using the Low Resolution Imaging Spectrometer (LRIS; Oke et al. 1995) and the DEep Imaging Multi-Object Spectrograph (DEIMOS; Faber et al. 2003). We observed three Keck slitmasks in the COSMOS field. On UT 2010 March 12 we observed `cos10b` for 5200 s using the dual-beam LRIS instrument. We used the 400 ℓ mm^{-1} grism on the blue arm of the spectrograph (blazed at 3400 Å; resolving power $R \equiv \lambda/\Delta\lambda \sim 600$), the 400 ℓ mm^{-1} grating on the red arm of the spectrograph (blazed at 8500 Å; $R \sim 700$), and 6800 Å dichroic. On UT 2010 March 13 we observed `cos10a` for 1200 s using LRIS. The red CCD was non-functional that night, so we channeled all of the light to the blue arm of the spectrograph and again used the 400 ℓ mm^{-1} grism blazed at 3400 Å. On UT 2010 March 14 we observed `cos10d` for 3600 s with DEIMOS in cloudy conditions, using the 600 ℓ mm^{-1} grating (blazed at 7500 Å; $R \sim 1600$) and the 4000 Å order-blocking filter. Masks all used $\sim$1.″2 wide slitlets. Data reduction followed standard procedures, and we flux calibrated the data using observations of standard stars from Massey & Gronwall (1990). Note that the DEIMOS data were taken in non-photometric conditions, resulting in an uncertainty in the flux scale of those sources.

Target selection was done prior to access to the *WISE* data in the COSMOS field, though we had already anticipated that red $W1-W2$ colors would be an effective method to identify a large population of AGNs. We sought to test that hypothesis using *Spitzer*/IRAC imaging from the S-COSMOS survey (Sanders et al. 2007), assuming that $W1 \sim [3.6]$ and $W2 \sim [4.5]$. Additional targets were selected using the Stern et al. (2005) IRAC AGN wedge selection criteria. Figure 17 and Table 3 present the results for the six COSMOS targets that subsequently were found to match our $W1 - W2 \geqslant 0.8$ AGN candidate selection criterion. All six would also be selected by the Stern et al. (2005) IRAC criteria. Table 4 in the Appendix presents the results for the additional COSMOS targets observed on these masks. Our new Keck results are occasionally slightly discrepant with previous results, but typically with $\Delta z \leqslant 0.01$. The S/N of these new data are quite high and the data were taken at relatively high spectral dispersion, suggesting that these redshifts should take precedence over previous results.

Four of the sources show prominent AGN features, such as broadened Mg II 2800 emission. WISE J100036.06+022830.5 does not show obvious AGN features; the spectrum shows narrow emission lines from [O II], [Ne III], Hβ, and [O III], as well as Balmer absorption lines indicative of a relatively young stellar

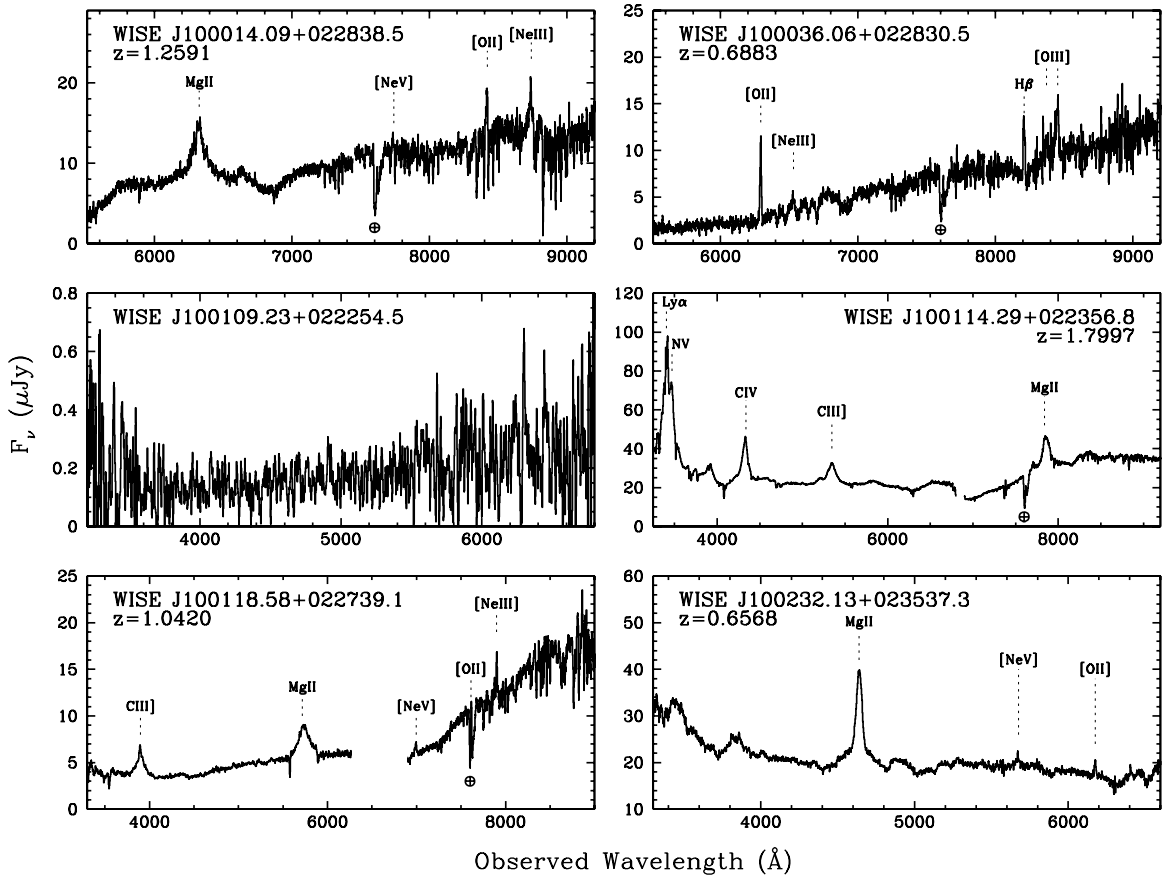

Figure 17. Results from Keck spectroscopy of sources identified as AGN candidates based on their *WISE* colors, obtained in 2010 March. All six sources here are also selected as AGN candidates based on their *Spitzer*/IRAC colors (Stern et al. 2005). Prominent emission lines are marked, as is the telluric A-band absorption at 7600 Å. DEIMOS spectra (see Table 3) were obtained in non-photometric conditions; the relative calibration of such sources should be reliable, though the absolute scale is uncertain.

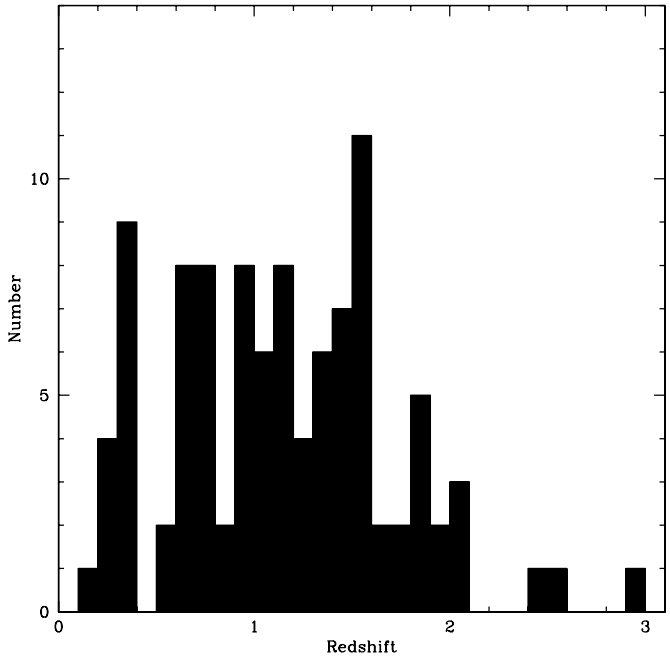

Figure 18. Histogram of spectroscopic redshifts for *WISE*-selected AGN candidates in the COSMOS field. Of the 130 such candidates, 101 have spectroscopic redshifts. The median redshift is $\langle z \rangle = 1.11$.

population. We find $\log([\mathrm{O\,III}]/\mathrm{H}\beta) \sim 0.12$, which is consistent with both star-forming and AGN activity in the Baldwin et al. (1981) diagram; spectral features redward of our data are required to distinguish the principle line excitation mechanism. We did not obtain a redshift for WISE J100109.23+022254.5 with our data, though Brusa et al. (2010) identify this source as a narrow-lined AGN $z = 1.582$ on the basis of their deep Keck/DEIMOS spectroscopy; the quality of the redshift is not indicated. Our spectroscopy does not show any features such as redshifted C IV emission or absorption to confirm that redshift. However, we note that strongest feature at this redshift is likely to be [O II] emission at 9623 Å. This is beyond the wavelength coverage of our Keck spectroscopy.

Figure 18 presents the distribution of spectroscopic redshifts for the *WISE* AGN candidates. We have spectroscopic redshifts for 101 of the 130 candidates (72%); the median redshift is $\langle z \rangle = 1.11$. Seven of these candidates are from outside the IRAC AGN wedge, four of which have spectroscopic redshifts. Two are broad-lined quasars at $z \sim 1$; the other two are galaxies at $z = 0.27$ and $z = 0.75$ from zCOSMOS. This suggests that the 95% reliability rate derived in Section 3.1 is actually a lower limit; some of the *WISE*-selected candidates are indeed AGNs despite not being identified as such by their IRAC colors.

4. CONCLUSIONS

We use the deep, public, multiwavelength data in the ~ 2 deg^2 COSMOS survey to motivate a very simple, empirical mid-infrared criterion to identify AGN candidates with the *WISE* satellite. Selecting sources with $W1 - W2 \geqslant 0.8$ identifies 61.9 ± 5.4 AGN candidates per deg^2 at the 10σ depth of the

WISE COSMOS data (e.g., 160 μJy at 4.6 μm). Using deep *Spitzer* data in this field and adopting the mid-infrared two-color AGN selection criteria of Stern et al. (2005) as the truth sample, this simple *WISE* color cut is approximately 78% complete and 95% reliable at identifying AGNs. Of the seven "contaminants" in the COSMOS field identified as AGN candidates using our new *WISE* color criterion but not selected as an AGN candidate from the *Spitzer* color criteria, two are identified as broad-lined quasars, implying that the reliability of this simple color selection is better than 95% at the depth of the *WISE* COSMOS observations, $W2 \sim 15.0$. We caution, however, that COSMOS, by design, is at very low ecliptic latitude implying that its *WISE* coverage is shallower than average. In deeper *WISE* fields, this simple color cut suffers more contamination. Here, we show that the combined criteria $W1 - W2 \geqslant 0.8$ and $W2 \leqslant 15$ robustly identifies an extremely robust, highly complete AGN sample. In Assef et al. (2012), we use the deeper, wider-area Boötes field to derive a $W2$-dependent AGN color selection criterion that is applicable in deeper areas of the *WISE* all-sky survey.

Forty-six of the *WISE*-selected AGN candidates in the COSMOS field are known broad-lined quasars previously identified by the SDSS (e.g., 21.9 type-1 quasars per deg^2). The median optical-to-mid-IR color of these type-1 AGN is $\langle i - W2 \rangle = 4.75$. The 10σ $W2$ depth that we applied to the *WISE* COSMOS observations corresponds to $W2 = 15.05$, implying that our mid-IR *WISE* AGN selection should identify unobscured quasars to an optical magnitude of $i \sim 19.8$. Richards et al. (2006b) combine the SDSS and 2QZ/6QZ quasar surveys to study the demographics and evolution of quasars below the SDSS photometric limits. They find $\sim$20 type-1 quasars per deg^2 to this depth. Assuming that the other $\sim$40 *WISE*-selected AGN candidates per deg^2 are type-2 quasars, the implied obscured-to-unobscured ratio is $\sim$2:1 at these bright depths. This result is in-line with expected ratios required to explain the intensity and hardness of the cosmic X-ray background (e.g., Treister et al. 2004; Treister & Urry 2005; Gilli et al. 2007; Ballantyne et al. 2011).

All of the *WISE*-selected AGN candidates in COSMOS have optical identifications. Approximately half are spatially resolved. *WISE*-selected AGNs tend to be among the optically faintest *WISE* sources, accounting for essentially none of the *WISE* sources brighter than $r = 18$, $\sim$20% of *WISE* sources at $r = 21$, and rising to $>$50% of sources fainter than $r = 23$. The r-band distribution of *WISE*-selected AGN candidates peaks at $r \sim 19.5$, but has a significant tail to fainter magnitudes. Considering the 101 candidates with spectroscopic redshifts, the median redshift is $\langle z \rangle = 1.11$.

Most ($\sim$75%) of the robust *WISE* AGN candidates covered by the deep *Chandra* and *XMM-Newton* imaging of COSMOS are detected at X-ray energies, while few of the expected contaminants are. Of particular note is the $\sim$25% of robust AGN candidates identified in 90 s *WISE* full-sky images that are missed in extremely deep, 60+ ks pencil-beam surveys by these flagship-class soft ($\lesssim$10 keV) X-ray missions. Such sources are expected to be heavily obscured, luminous, Compton-thick AGNs. In the next year, the *NuSTAR* satellite will map the COSMOS field in the 5–80 keV hard X-ray energy range, reaching depths $\sim$200 times more sensitive than previous surveys in this energy range. We expect that several of the obscured *WISE* AGN candidates will be detected by *NuSTAR*.

The 130 *WISE*-selected AGN candidates identified in the COSMOS field are sufficiently large to characterize general properties of the population, and the expectation is that this selection criterion will be valuable for a wide range of future studies, such as understanding the energetics of sources identified at other wavelengths (e.g., Bond et al. 2012), comparing the environments of type 1 and type 2 AGNs, and probing the role of AGNs in galaxy formation and evolution. A companion paper, Assef et al. (2012), uses nearly an order of magnitude larger sample of *WISE*-selected AGNs in the $\sim$10 deg^2 Boötes field to study the evolutionary properties of this population.

We gratefully acknowledge the anonymous referee for helpful comments that have made the paper both clearer and stronger. We also thank P. Capak for providing two unpublished redshifts obtained with DEIMOS. This publication makes use of data products from the *Wide-field Infrared Survey Explorer*, which is a joint project of the University of California, Los Angeles, and the Jet Propulsion Laboratory/California Institute of Technology, funded by the National Aeronautics and Space Administration. We gratefully acknowledge the COSMOS survey and are thankful for the extensive and high quality data products that they have publicly released. This publication makes use of data obtained at the Keck Observatory. The authors wish to recognize and acknowledge the very significant cultural role and reverence that the summit of Mauna Kea has always had within the indigenous Hawaiian community; we are most fortunate to have the opportunity to conduct observations from this mountain. SDSS is funded by the Alfred P. Sloan Foundation, the Participating Institutions, the National Science Foundation, the U.S. Department of Energy, the National Aeronautics and Space Administration, the Japanese Monbukagakusho, the Max Planck Society, and the Higher Education Funding Council for England. This research has made use of the NASA/IPAC Infrared Science Archive (IRSA), which is operated by the Jet Propulsion Laboratory, California Institute of Technology, under contract with the National Aeronautics and Space Administration. This work is based in part on observations made with the *Spitzer Space Telescope*, which is operated by the Jet Propulsion Laboratory/California Institute of Technology, under a contract with NASA. This work is also based in part on observations made with the NASA/ESA *Hubble Space Telescope*, obtained at the Space Telescope Science Institute, which is operated by the Association of Universities for Research in Astronomy, Inc., under NASA contract NAS 5-26555. R.J.A. is supported by an appointment to the NASA Postdoctoral Program at the Jet Propulsion Laboratory, administered by Oak Ridge Associated Universities through a contract with NASA.

APPENDIX

ADDITIONAL SPECTROSCOPIC REDSHIFTS IN THE COSMOS FIELD

The three slitmasks that we observed were designed to target *WISE*-selected AGN candidates in the COSMOS field, though the low source density of such sources allowed for additional spectroscopic targets. We primarily filled out the masks with IRAC-selected AGN candidates, using the two-color criteria of Stern et al. (2005). Given the interest and use of the COSMOS field by a broad community, we include those additional sources here.

Table 4 presents the results for 26 COSMOS sources for which we obtained redshifts; the six targeted sources are listed in Table 3. We include the quality ("Q") of each spectroscopic redshift. Quality flag "A" signifies an unambiguous redshift determination, typically relying upon multiple emission or

Table 4
Additional Results from Keck Observations

I_{814}	R.A.	Decl.	z	Q	Slitmask(s)	Notes
17.32	10:00:11.83	+02:26:23.1	0.440	A	D[35]	[O II], [Ne III], Hζ, Hϵ, Hδ, Hγ, Hβ, [O III]
16.26	10:00:14.89	+02:27:17.9	0.728	A	D[38]	[O II], Hβ, [O III]
19.30	10:00:22.79	+02:25:30.6	0.349	A	D[3]	CaHK, Hα, [N II]
17.99	10:00:24.28	+02:27:36.2	1.243	B	D[39]	[O II]
17.14	10:00:24.51	+02:26:18.1	1.129	A	D[34]	[O II]
18.36	10:00:28.56	+02:27:25.8	0.248	A	D[4]	CaH, Hγ, Hβ, [O III], Hα, [N II]
17.15	10:00:29.55	+02:26:35.9	0.348	B	D[36]	[O II], Hβ, [O III], Hα, [N II] (could be serendip)
16.93	10:00:32.46	+02:27:59.3	1.405	B	D[41]	[O II]
16.80	10:00:33.23	+02:27:59.3	0.981	B	D[42]	[O II]
17.93	10:00:44.50	+02:23:54.0	1.299	B	D[17]	[O II], CaHK
18.43	10:00:50.15	+02:26:18.5	3.730	A	D[33]	QSO: Lyα,C IV
18.56	10:00:50.58	+02:23:29.3	3.093	A	D[13]	QSO: Lyα,C IV, C III]
19.08	10:00:56.65	+02:26:35.5	0.344	A	B, D[0]	Mg II absn,[O II], CaH, Hγ, Hβ, [O III], Hα, [N II]
17.55	10:00:58.07	+02:26:16.8	0.425	A	D[32]	[O II], Hβ, [O III], Hα
16.55	10:00:58.70	+02:25:56.2	0.694	A	D[28]	QSO: [Ne V], [O II], Hβ, [O III]
17.09	10:00:59.00	+02:24:17.9	1.193	B	B	[O II]
19.15	10:00:59.81	+02:24:30.7	0.541	A	B	[O II]
16.94	10:01:08.35	+02:23:42.0	1.930	A	B, D[15]	QSO: Lyα,C IV, C III],Mg II
18.22	10:01:08.65	+02:23:14.1	0.503	A	D[12]	[O II], D4000
16.52	10:01:13.93	+02:25:48.1	0.373	A	B	QSO: broad Mg II,[Ne V], [O II], Hα
17.18	10:01:14.68	+02:24:49.5	1.656	A	B	LBG: C II, C IV,[O II]
16.36	10:01:17.00	+02:27:31.2	0.518	A	B	Hα
16.25	10:02:17.42	+02:29:59.7	1.100	A	A	QSO: C IV, C III]; odd broad lines at $\sim$1650 Å
17.56	10:02:28.18	+02:30:15.4	0.344	B	A	[O II]
15.23	10:02:29.89	+02:32:25.1	0.431	A	A	AGN: [Ne V], [O II], [Ne III], [O III]
17.76	10:02:31.90	+02:35:07.4	0.880	A	A	AGN: C III],Mg II

Notes. Q indicates the quality of the redshift (see text for details). Masks A and B were observed with LRIS. Mask D was observed with DEIMOS; the bracketed numbers indicate the DEIMOS slitlet number.

absorption features. Quality flag "B" signifies a less certain redshift determination, such as the robust detection of an isolated emission line, but where the identification of the line is uncertain (e.g., Stern et al. 2000a). Quality flag "B" might also be assigned to a source with a robust redshift identification, but where some uncertainty remains as to the astrometric identity of that spectroscopic source. We consider the quality "B" results likely to be correct, but additional spectroscopy would be beneficial. All of the spectroscopic redshifts in Table 3 are of quality "A."

REFERENCES

Abazajian, K., Adelman-McCarthy, J. K., Agüeros, M. A., et al. 2004, AJ, 128, 502
Abazajian, K., Adelman-McCarthy, J. K., Agüeros, M. A., et al. 2009, ApJS, 182, 543
Ajello, M., Greiner, J., Sato, G., et al. 2008, ApJ, 689, 666
Alexander, D. M., Bauer, F. E., Brandt, W. N., et al. 2003, AJ, 126, 539
Alonso-Herrero, A., Pérez-González, P. G., Alexander, D. M., et al. 2006, ApJ, 640, 167
Ashby, M. L. N., Stern, D., Brodwin, M., et al. 2009, ApJ, 701, 428
Assef, R. J., Kochanek, C. S., Ashby, M. L. N., et al. 2011, ApJ, 728, 56
Assef, R. J., Kochanek, C. S., Brodwin, M., et al. 2010, ApJ, 713, 970
Assef, R. J., et al. 2012, ApJ, submitted
Baldwin, J. A., Phillips, M. M., & Terlevich, R. 1981, PASP, 93, 5
Ballantyne, D. R., Draper, A. R., Madsen, K. K., Rigby, J. R., & Treister, E. 2011, ApJ, 736, 56
Barmby, P., Alonso-Herrero, A., Donley, J. L., et al. 2006, ApJ, 642, 126
Bassani, L., Dadina, M., Maiolino, R., et al. 1999, ApJS, 121, 473
Blain, A., et al. 2012, ApJ, submitted
Bond, N. A., Benford, D. J., Gardner, J. P., et al. 2012, ApJ, 750, L18
Bondi, M., Ciliegi, P., Schinnerer, E., et al. 2008, ApJ, 681, 1129
Bovy, J., Hennawi, J. F., Hogg, D. W., et al. 2011, ApJ, 729, 141
Brandt, W. N., & Hasinger, G. 2005, ARA&A, 43, 827
Bridge, C. R., Blain, A., Borys, C. J. K., et al. 2012, ApJL, submitted (arXiv:1205.4030)
Brusa, M., Civano, F., Comastri, A., et al. 2010, ApJ, 716, 348
Brusa, M., Fiore, F., Santini, P., et al. 2009, A&A, 507, 1277
Burningham, D., Ajello, M., Greiner, J., et al. 2011, ApJ, 728, 58
Capak, P., Aussel, H., Ajiki, M., et al. 2007, ApJS, 172, 99
Cardamone, C. N., Urry, C. M., Damen, M., et al. 2008, ApJ, 680, 130
Cardelli, J. A., Clayton, G. C., & Mathis, J. S. 1989, ApJ, 345, 245
Comastri, A., Ranalli, P., Iwasawa, K., et al. 2011, A&A, 526, 9
Comastri, A., Setti, G., Zamorani, G., & Hasinger, G. 1995, A&A, 296, 1
Cushing, M. C., Kirkpatrick, J. D., Gelino, C. R., et al. 2011, ApJ, 743, 50
D'Abrusco, R., Massaro, F., Ajello, M., et al. 2012, ApJ, 748, 68
De Breuck, C., Seymour, N., Stern, D., et al. 2010, ApJ, 725, 36
Dey, A., Soifer, B. T., Desai, V., et al. 2008, ApJ, 677, 943
Donley, J., Rieke, G. H., González, P. G., Rigby, J. R., & Alonso-Herrero, A. 2007, ApJ, 660, 167
Donley, J., Rieke, G. H., González, P. G., Rigby, J. R., & Alonso-Herrero, A. 2008, ApJ, 687, 111
Donley, J. L., Koekemoer, A. M., Brusa, M., et al. 2012, ApJ, 748, 142
Donoso, E., Yan, L., Tsai, C., et al. 2012, ApJ, 748, 80
Eckart, M., McGreer, I., Stern, D., Harrison, F., & Helfand, D. 2010, ApJ, 708, 584
Edelson, R., & Malkan, M. A. 2012, ApJ, 751, 52
Eisenhardt, P. R. M., Brodwin, M., Gonzalez, A. H., et al. 2008, ApJ, 684, 905
Eisenhardt, P. R. M., Griffith, R. L., Stern, D., et al. 2010, AJ, 139, 2455
Eisenhardt, P. R. M., Stern, D., Brodwin, M., et al. 2004, ApJS, 154, 48
Eisenhardt, P. R. M., Wu, J., Tsai, C.-W., et al. 2012, ApJ, submitted
Elvis, M., Civano, F., Vignali, C., et al. 2009, ApJS, 184, 158
Faber, S. M., Phillips, A. C., Kibrick, R. I., et al. 2003, Proc. SPIE, 4841, 1657
Faure, C., Kneib, J.-P., Covone, G., et al. 2008, ApJS, 176, 19
Fazio, G. G., Hora, J. L., Allen, L. E., et al. 2004, ApJS, 154, 10
Fiore, F., Grazian, A., Santini, P., et al. 2008, ApJ, 672, 94
Fiore, F., Puccetti, S., Brusa, M., et al. 2009, ApJ, 693, 447
Frayer, D. T., Sanders, D. B., Surace, J. A., et al. 2009, AJ, 138, 1261
Gabor, J. M., Impey, C. D., Jahnke, K., et al. 2009, ApJ, 691, 705
Galametz, A., Stern, D., De Breuck, C., et al. 2012, ApJ, 749, 169
Gilli, R., Comastri, A., & Hasinger, G. 2007, A&A, 463, 79
Gordon, K. D., & Clayton, G. C. 1998, ApJ, 500, 816
Gorjian, V., Brodwin, M., Kochanek, C. S., et al. 2008, ApJ, 679, 1040
Gregg, M. D., Becker, R. H., White, R. L., et al. 1996, AJ, 112, 407
Griffith, R. L., & Stern, D. 2010, AJ, 140, 533

Harrison, F. A., Boggs, S., Christensen, F., et al. 2010, Proc. SPIE, 7732, 773205
Hasinger, G., Cappelluti, N., Brunner, H., et al. 2007, ApJS, 172, 29
Hatziminaoglou, E., Fritz, J., Franceschini, A., et al. 2008, MNRAS, 386, 1252
Hickox, R. C., Jones, C., Forman, W. R., et al. 2007, ApJ, 671, 1365
Hickox, R. C., Jones, C., Forman, W. R., et al. 2009, ApJ, 696, 891
Hickox, R. C., Myers, A. D., Brodwin, M., et al. 2011, ApJ, 731, 117
Hopkins, P. F., Hernquist, L., Cox, T. J., & Kereš, D. 2008, ApJS, 175, 356
Jackson, N. 2008, MNRAS, 389, 1311
Jarrett, T. H., Cohen, M., Masci, F., et al. 2011, ApJ, 735, 112
Kirkpatrick, J. D., Cushing, M. C., Gelino, C. R., et al. 2011, ApJS, 197, 19
Koekemoer, A. M., Aussel, H., Calzetti, D., et al. 2007, ApJS, 172, 196
Komiyama, Y., Miyazaki, S., Yagi, M., et al. 2003, Proc. SPIE, 4841, 152
Lacy, M., Petric, A. O., Sajina, A., et al. 2007, AJ, 133, 186
Lacy, M., Storrie-Lombardi, L. J., Sajina, A., et al. 2004, ApJS, 154, 166
Lilly, S. J., Le Fèvre, O., Renzini, A., et al. 2007, ApJS, 172, 70
Mainzer, A. K., Eisenhardt, P., Wright, E. L., et al. 2005, Proc. SPIE, 5899, 262
Maiolino, R., Marconi, A., Salvati, M., et al. 2001, A&A, 365, 28
Mancone, C. L., Gonzalez, A. H., Brodwin, M., et al. 2010, ApJ, 720, 284
Martínez-Sansigre, A., Rawlings, S., Bonfield, D. G., et al. 2007, MNRAS, 379, 6
Martínez-Sansigre, A., Rawlings, S., Lacy, M., et al. 2006, MNRAS, 370, 1479
Massaro, F., D'Abrusco, R., Tosti, G., et al. 2012, ApJ, 750, 35
Massey, P., & Gronwall, C. 1990, ApJ, 358, 344
Matthews, T. A., Morgan, W. W., & Schmidt, M. 1964, ApJ, 140, 35
McCarthy, P. J., van Breugel, W., Spinrad, H., & Djorgovski, S. 1987, ApJ, 321, 29
Mortlock, D. J., Warren, S. J., Venemans, B. P., et al. 2011, Nature, 474, 616
Mullaney, J. R., Alexander, D. M., Goulding, A. D., & Hickox, R. C. 2011, MNRAS, 414, 1082
Oke, J. B., Cohen, J. G., Carr, M., et al. 1995, PASP, 107, 375
Palanque-Delabrouille, N., Yeche, C., Myers, A. D., et al. 2011, A&A, 530, 122
Papovich, C. 2008, ApJ, 676, 206
Park, S. Q., Barmby, P., Willner, S. P., et al. 2010, ApJ, 717, 1181
Polletta, M., Wilkes, B. J., Siana, B., et al. 2006, ApJ, 642, 673
Predehl, P., Böhringer, H., Brunner, H., et al. 2010, in AIP Conf. Proc. 1248, X-ray Astronomy 2009: Present Status, Multi-wavelength Approach and Future Perspectives, ed. A. Comastri, L. Angelini, & M. Cappi (Melville, NY: AIP), 543
Prescott, M. K. M., Impey, C. D., Cool, R. J., & Scoville, N. Z. 2006, ApJ, 644, 100
Reach, W. T., Megeath, S. T., Cohen, M., et al. 2005, PASP, 117, 978
Richards, G. T., Fan, X., Newberg, H. J., et al. 2002, AJ, 123, 2945
Richards, G. T., Lacy, M., Storrie-Lombardi, L. J., et al. 2006a, ApJS, 166, 470
Richards, G. T., Strauss, M. A., Fan, X., et al. 2006b, AJ, 131, 2766
Rieke, G. H., Young, E. T., Engelbracht, C. W., et al. 2004, ApJS, 154, 25
Rigopoulou, D., Mainieri, V., Almaini, O., et al. 2009, MNRAS, 400, 1199
Sanders, D. B., Salvato, M., Aussel, H., et al. 2007, ApJS, 172, 86
Schinnerer, E., Sargent, M. T., Bondi, M., et al. 2010, ApJS, 188, 384
Schinnerer, E., Smolčić, V., Carilli, C. L., et al. 2007, ApJS, 172, 46
Schmidt, M., & Green, R. F. 1983, ApJ, 269, 352
Scoville, N., Abraham, R. G., Aussel, H., et al. 2007, ApJS, 172, 38
Seymour, N., Stern, D., De Breuck, C., et al. 2007, ApJS, 171, 353
Silk, J., & Rees, M. J. 1998, A&A, 331, 1
Stern, D., Bunker, A. J., Spinrad, H., & Dey, A. 2000a, ApJ, 537, 73
Stern, D., Djorgovski, S. G., Perley, R., de Carvalho, R., & Wall, J. 2000b, AJ, 119, 1526
Stern, D., Eisenhardt, P., Gorjian, V., et al. 2005, ApJ, 631, 163
Stern, D., Kirkpatrick, J. D., Allen, L. E., et al. 2007, ApJ, 663, 677
Stern, D., Moran, E. C., Coil, A. L., et al. 2002a, ApJ, 568, 71
Stern, D., Tozzi, P., Stanford, S. A., et al. 2002b, AJ, 123, 2223
Treister, E., & Urry, C. M. 2005, ApJ, 630, 115
Treister, E., Urry, C. M., Chatzichristou, E., et al. 2004, ApJ, 616, 123
Trump, J. R., Impey, C. D., Elvis, M., et al. 2009, ApJ, 696, 1195
Trump, J. R., Impey, C. D., McCarthy, P. J., et al. 2007, ApJS, 172, 383
Tueller, J., Mushotzky, R. F., Barthemy, S., et al. 2008, ApJ, 681, 113
Vignali, C., & Comastri, A. 2002, A&A, 381, 834
Wright, E. L., Eisenhardt, P. R. M., Mainzer, A. K., et al. 2010, AJ, 140, 1868
Wu, J., Tsai, C.-W., Sayers, J., et al. 2012, ApJ, submitted
Yan, L., et al. 2012, ApJ, submitted
York, D. G., Khare, P., Vanden, B. D., et al. 2006, MNRAS, 367, 945
Zakamska, N. L., Strauss, M. A., Heckman, T. M., et al. 2004, AJ, 128, 1002
Zirm, A. W., Dickinson, M., & Dey, A. 2003, ApJ, 585, 90